This thesis was typeset with LaTeX, using a modified version of the University of California Ph.D. dissertation class file, `ucthesis.cls`. Unless otherwise noted, all figures in this thesis were created by the author using TECPLOT 10® or PAINT Software®.

The Earth's Slichter modes

Michel Nzikou Mamboukou

B.Sc., Marien Ngouabi University, 2004
Honours (Maitrise) in Physics, Marien Ngouabi University, 2006
Postgraduate Diploma in Mathematical Sciences, AIMS, 2008
M.Sc. Physics (Material Science), University of Cape Town, 2011

A Thesis
Submitted to the School of Graduate Studies
of the University of Lethbridge
in Partial Fulfilment of the
Requirements of the Degree

MASTER OF SCIENCE

Department of Physics & Astronomy
University of Lethbridge
Lethbridge, Alberta, Canada

Dedication

This thesis is dedicated to my late parents.

Abstract

Numerical methods have been used to predict the eigenperiods and eigenfunctions of the Earth's Slichter modes, known as the Slichter triplets. In order to test the validity of our method, we have also computed the frequencies and displacement eigenfunctions of some of the inertial modes of the Earth's fluid core. We use a Galerkin method to integrate the Three Potential Description (3PD) for a neutrally, stratified and rotating fluid core of a modified Preliminary Reference Earth Model (PREM). Moreover, the same mathematical tool is used for the computation of the frequencies and displacement amplitudes of the Slichter modes. In the Galerkin formulation of the 3PD, using the divergence theorem, we make use of the natural character of the boundary conditions to reduce the order of derivatives from second to first. To compute the frequencies of the Slichter modes, we solve simultaneously the equations of the inner core motion and the dynamics of the fluid core as described above. The results are compared to those in previous studies and it is shown that in the case of the inertial modes they agree well, which proves the validity of the approach. For the Slichter modes, however, it is shown that the results are significantly different from previous work for a similar Earth model. We have also plotted the displacement eigenfunctions for the motion of the fluid in the fluid core during the Slichter oscillations. It is shown that the pattern of motion is consistent with the motion of the inner core, which serves as a second test of the validity of our results.

Acknowledgements

I would like to thank my supervisor Dr. Seyed-Mahmoud for affording me an opportunity to study at the University of Lethbridge. I have been blessed to have a supervisor who cares about my work and whose critical constructive criticism of my work has made me a better Physicist, particularly in Computational Geophysics. When I joined the Geophysics Group at the University of Lethbridge, my knowledge of programming was limited to standard programming in various languages such as Python, Sage, R, Turtle, Turbo, Qbasic, Matlab, and Fortran. I am grateful to my supervisor Dr. Seyed-Mahmoud for the intense training in modelling techniques using FORTRAN in which I have become so confident.

I would also like to thank my supervisory committee members, Dr. Mark Walton and Dr. Marc R. Roussel for sparing time to have meetings during the course of this work for the past two years. I thank you all for the constructive suggestions and encouragements. I would like to thank the rest of the staff of the Physics Department and my research mate Ali Moradi for constructive discussions and encouragements. When I joined the Department of Physics at the University of Lethbridge, I felt welcomed, and will always cherish the nice working environment.

Lastly, I would like to thank the administration staff for helping me in various ways during the last two years. I say thank you to Laurie Scott for the good job she is doing, and to the staff of the SGS for being cheerful and for the encouragements.

This research was supported by NSERC Discovery Grant No. 600001586 awarded to Dr. Seyed-Mahmoud, and by the School of Graduate Studies.

Contents

List of Tables

List of Figures

List of Abbreviations

3PD	Three Potential Description.
CMB	Core Mantle Boundary.
FC	Fluid Outer Core.
IC	Inner Core.
ICB	Inner Core Bounday.
IMSL	International Mathematics and Statistics Library.
P	Principal.
PDE	Partial Differential Equation.
PREM	Preliminary Reference Earth Model.
S	Secondary.
SSA	Subseismic Approximation.
SSWE	Subseismic Wave Equation.
TPD	Two Potential Description.

Chapter 1

Introduction

1.1 Motivation

Referred as the blue planet, the Earth is the densest and the fifth largest of the eight planets in the solar system, and the third planet from the Sun [1]. Its rich physical and geological properties are the key for sustaining life since its origin [2]. The Earth is composed of three major layers: a solid Inner Core (IC) with radius $R_{IC} = 1221.5$ km, the Fluid Outer Core (FC) which is responsible for most of the Earth's magnetic field, and about 2258.5 km in thickness, and finally a thick layer of solid mantle with thickness of about 2891 km. In addition, the Earth's mean radius measured from the geocentre to the surface is $R = 6371$ km [3, 4]. Besides the above physical properties, the Earth is chemically composed of iron (32.1%), oxygen (30.1%), silicon (15.1%), magnesium (13.9%), sulfur (2.9%), nickel (1.8%), calcium (1.5%), and aluminum (1.2%) and 1.2% for other trace elements. However, due to mass segregation, the Earth's core known as the inner core plus the fluid core is mostly composed of iron (88.8%), and a small amount of nickel (5.8%), sulfur (4.5%), and about

1% of trace elements [5]. In most studies, the Earth has been approximated as a sphere, while its true figure is close to an oblate spheroid, flattened along the polar axis so that there is a bulge at the equator due to rotation, and, as a consequence the equatorial radius ($R_e = 6378.1$ km) is about 21 km longer than the polar radius ($R_p = 6356.8$ km), and the flattening produces an ellipticity of about $e = 0.0033528$ at the surface [3, 4, 6, 7].

The objectives of this work are to predict the frequencies and the displacement eigenfunctions of the small translational oscillations of the inner core known as the Slichter modes. Known as the hottest layer of the Earth, the inner core is the most enigmatic and remote part of our Earth. It was discovered in 1936 by Inge Lehmans from Denmark, using early seismological observations of P-waves travelling through the Earth's deep interior [8,9]. The inner core crystallization from the center outward is believed to originate from the increase in pressure as we go deeper toward the center due to mass, and also because iron can no longer be liquid above a certain pressure [10, 11]. Moreover, due to the temperature drops below the melting point of the inner core boundary, the inner core crystallyzes within the liquid outer core [10–12].

The inner core is mostly composed of iron and nickel, and the evidence from earthquake seismology that P-waves travel through both solid and liquid whereas S-waves only travel through solid, revealed the solid aspect of the inner core [10]. P-waves are compressional waves and are Principal (P) waves to be recorded at the seismograph stations at the Earth's surface, and they are longitudinal in nature (top image in figure 1). However, S-waves are Secondary (S) waves and are recorded after the P-waves, they are shear waves and are transverse in nature and they displace the ground perpendicular to the direction of

Figure 1.1: P (Principal) and S (Secondary) wave representations from Earthquake and Seismic Education notes [15]

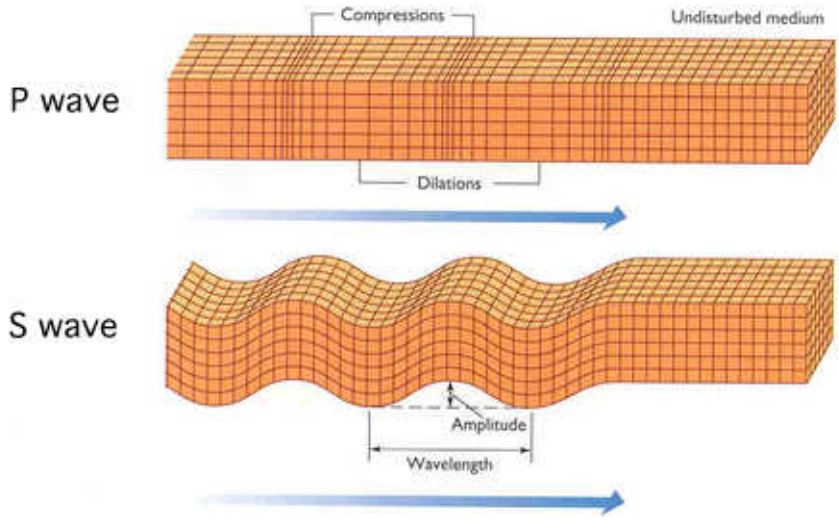

propagation during an earthquake excitation (bottom image in figure 1) [13, 14]. Since the core is not directly accessible, much is still unknown about its properties. However, most of the information extracted from the Earth has been made possible through ray seismology and the normal mode theory. The velocity of the P and S-waves are given as

$$v_p = \sqrt{\frac{\lambda + 2\mu}{\rho}}$$

$$v_s = \sqrt{\frac{\mu}{\rho}}$$

where λ, μ and ρ are the Lamé parameter, the shear modulus, and the density of the media respectively. The above parameters in the core are established through the observations of seismology and also the free oscillations. However, the density jump near the inner core boundary is poorly known and varies from one model to another.

The spectrum of the Earth's free oscilllations is divided into five types according to the normal mode theory:

1- the seismic oscillations with the elasticity as their restoring force which have periods shorter than a few hours;

2-the gravity modes which are excited in any unstably stratified region of the Earth's fluid core;

3-the Earth's wobble and nutation modes caused by the Earth's rotation and flattened figure;

4- the inertial modes of the Earth's fluid core caused by the Earth's rotation;

5-the translational modes of the solid inner core, known as the Slichter modes, with the gravity as their restoring force.

The periods of some of the Earth's modes depend on the material properties of the Earth's interior. If one of the modes is detected, the frequency, and the shape of the predicted mode may be used to extract much information about the Earth's interior. Hundreds of oscillations of type 1 have been detected and used to improve the existing Earth models (e.g PREM, by Dziewonsky and Anderson, 1981) [16]. Chandler (1891) discovered, from available astronomical data, one of the Earth's wobble modes, known as the Chandler wobble, which has a period of about 430 days. Therefore any reliable Earth model must yield a wobble period in the vicinity of the period of the Chandler wobble.

It is commonly accepted that the Earth has been existed for at least 3.6 billion years [17]. The source and origin of its magnetic field is one of the most interesting topics in the study of the Earth. The two dominant theories attempting to explain the Earth's magnetic field are based on precession driven flow and thermal convection. However, it was

shown that these ideas were insufficient to fully explain the origin, and the polarity reversal of the Earth's magnetic field [18, 19]. The determination of important parameters of the Earth such as the density jump near the Inner Core Bounday (ICB), may help explain the growth of the inner core (IC) from the outer fluid core [20, 21] and also to understand the existence and the polarity reversal of the magnetic field [8].

The Earth's material properties, such as viscosity and the density jump near the ICB, are poorly constrained by seismology and the normal mode theory. Indeed a variety of Earth models such as the Preliminary Reference Earth Model (PREM) [16], CORE11 [22] and 1066A [23] give different density profiles, determined using surface observations of the seismic activity travelling back and forth through the Earth, and also the use of the normal modes. Therefore, for a better determination of the Earth's parameters, or for instance a direct image of the density structure inside the earth, it is necessary to develop methods which can be used to accurately predict the period of the Earth's long-period modes. Previous studies show the periods of the long-period modes such as the Slichter modes to depend on the inverse of the square root of the density difference across the ICB as $T \simeq k(\rho_{IC} - \rho_0)^{-1/2}$, where k depends on the dimensions and densities of the inner and outer cores, and ρ_{IC} and ρ_0 are the densities of the inner and outer cores near the inner core boundary respectively [24–26]. Therefore, with this direct dependence, the Slichter modes are the best candidates to estimate the density jump and other parameters such as the viscosity of the fluid core near the ICB, and maybe also to quantify the energy required to maintain the geodynamo of the Earth [27].

The inner core oscillates with the periods sensitive to the physical properties such as density of both the inner and fluid cores at the ICB. It is held inside the FC mainly by the buoyancy force [28]. Following the observations of unusual gravity signals recorded on the LaCoste-Romberg Earth tide gravimeter after the 1960 Chilean Earthquake, Slichter [29], based on his research on a particular types of oscillations known as S_1 (spheroidal oscillation), proposed that the observed unusual peak with a period of about 86 minutes could have been produced by the translational oscillations of the IC. Further research showed that the period of the central mode was much longer, 3-4 hours, and that the effects of the Earth's rotation and its ellipticity cause the principal mode (central mode) to split into three frequencies known as the Slichter triplet. Much effort has been made and is still ongoing to detect these modes [30, 31]. Although, there have been a few claims of the detection of these modes (to be discussed later in this section), there is still a concensus among researchers that much work is still needed [32–34].

In this work, we develop a method which we apply to a realistic Earth model to numerically predict the periods of the Earth's Slichter triplet. We will first test our computational codes by numerically solving for the frequencies and the displacement eigenfunctions of the inertial modes of a rotating and spherical Earth model with a compressible and neutrally stratified fluid core based on the PREM model with rigid inner core and mantle. Thereafter, we will numerically compute the eigenperiods and eigenfunctions of the Slichter modes for the same model. We will show the steps we have taken to make sure that the results are converged.

1.2 Fundamental Equations of the Fluid Core

A set of different methods have been so far used to study the normal modes of the Earth, from traditional approaches to the three potential description (3PD). In this section we will briefly review some of these methods. The 3PD will be discussed in chapter 2.

The Earth's liquid core is considered as inviscid, with the reference state being one of hydrostatic equilibrium in a coordinate system which is attached to the Earth and rotates with a constant angular velocity

$$\boldsymbol{\omega}_r = \Omega \widehat{\mathbf{e}}_{\mathbf{3}}$$

where Ω is the rate of rotation of the Earth and $\widehat{\mathbf{e}}_3$ is a unit vector along the rotational axis. In this reference frame the density, the pressure, and the gravity are labelled as ρ_0, p_0, and $\mathbf{g}_0$ and are related by [25, 35]

$$\nabla p_0 = \rho_0 \mathbf{g}_0 \tag{1.1}$$

$$\mathbf{g}_0 = \nabla W_0 \tag{1.2}$$

$$\nabla^2 W_0 = -4\pi G\rho_0 + 2\Omega^2 \tag{1.3}$$

$$\nabla \rho_0 = (1-\beta)\rho_0 \frac{g_0}{\alpha^2} \tag{1.4}$$

where W_0, G, α, β are respectively the gravitational potential, the constant of gravitation, the local compressional wave speed, and the stability parameter. The stability parameter is defined as

$$\beta = -\frac{\alpha^2 N^2}{g_0^2} \tag{1.5}$$

where N is the Brunt Väissäla frequency. The stability parameter measures the departure of the Earth's equilibrium density from neutral stratification. Specifically, its sign $\beta < 0$

($N^2 > 0$), $\beta = 0$ ($N^2 = 0$) or $\beta > 0$ ($N^2 < 0$) correspond to a stably, neutrally or unstably stratification. It is an important parameter for the understanding of Earth's geodynamo. However, like the density jump near the ICB, it has not been well defined [25, 35].

The conservation of mass, momentum, gravitational flux and entropy yield the equations governing small oscillations of an inviscid liquid core [36]:

$$\frac{\partial \rho_1}{\partial t} = -\nabla \cdot (\rho_0 \mathbf{v}) \tag{1.6}$$

$$\frac{\partial \mathbf{v}}{\partial t} + 2\Omega \widehat{e}_3 \times \mathbf{v} = -\frac{1}{\rho_0}\nabla p_1 + \nabla V_1 + \frac{\rho_1}{\rho_0}\mathbf{g}_0 \tag{1.7}$$

$$\nabla^2 V_1 = -4\pi G \rho_1 \tag{1.8}$$

$$\frac{\partial p_1}{\partial t} = \alpha^2 \frac{\partial \rho_1}{\partial t} - \beta \rho_0 \mathbf{v} \cdot \mathbf{g}_0 \tag{1.9}$$

where $\mathbf{v} = \frac{\partial \mathbf{u}}{\partial t}$, $\mathbf{u}$, ρ_1, p_1 and V_1, all regarded as first order departures from the equilibrium reference frame, are the velocity, the fluid displacement, the perturbation in density, the pressure disturbance and the perturbation in the gravitational potential. Here $\mathbf{u}$ is the Lagrangian displacement from the equilibrium configuration.

Since we are dealing with small oscillations, all the field variables have time dependence of $e^{i\omega t}$. With this consideration and some mathematical operations in the above equations, the fundamental dynamical equations are written as

$$\omega^2 \mathbf{u} - 2i\omega\Omega \widehat{e}_3 \times \mathbf{u} = \frac{1}{\rho_0}\nabla p_1 - \nabla V_1 + \frac{\mathbf{g}_0}{\rho_0}\nabla \cdot (\rho_0 \mathbf{u}) \tag{1.10}$$

$$\nabla^2 V_1 = -4\pi G \nabla \cdot (\rho_0 \mathbf{u}) \tag{1.11}$$

$$\frac{p_1}{\rho_0} = -(\alpha^2 \nabla \cdot \mathbf{u} + \mathbf{u} \cdot \mathbf{g}_0) \tag{1.12}$$

The above equations (1.10-1.12) represent five scalar differential equations describing the dynamics of the Earth's fluid core [37]. In the traditional approach, to solve the above equa-

tions for the modes of a spherical, symmetric and rotating Earth model, the field variables are represented in spherical polar coordinates by means of spherical harmonics.

$$V_1 = \sum_{m=-\infty}^{\infty} \sum_{n=|m|}^{\infty} \phi_n^m Y_n^m \tag{1.13}$$

$$p_1 = \sum_{m=-\infty}^{\infty} \sum_{n=|m|}^{\infty} \psi_n^m Y_n^m \tag{1.14}$$

$$\mathbf{u} = \sum_{m=-\infty}^{\infty} \sum_{n=|m|}^{\infty} \mathbf{S}_n^m + \mathbf{T}_n^m \tag{1.15}$$

$$\mathbf{S}_n^m = [u_n^m \widehat{\mathbf{r}} + r v_n^m \nabla] Y_n^m \tag{1.16}$$

$$\mathbf{T}_n^m = -t_n^m \widehat{\mathbf{r}} \times \nabla Y_n^m \tag{1.17}$$

$$Y_n^m = P_n^m(cos\theta) e^{im\phi} \tag{1.18}$$

where $\mathbf{S}_n^m$, and $\mathbf{T}_n^m$, are the spheroidal and toroidal components of $\mathbf{u}$, and u_n^m, v_n^m, t_n^m, ϕ_n^m, ψ_n^m are functions of the radial coordinate and P_n^m the associated Legendre function of degree n and azimuthal order m. The spheroidal oscillations are similar to the P-waves: long-period oscillations strongly affected by the gravity. However, the toroidal or torsional oscillations are waves in which the motion is parallel to the sphere's surface. Contrarily to the spheroidal modes, gravity does not influence these modes.

The traditional approach is an effective tool for the computation of short period free oscillations, which rely on heavy truncations of the degree n of the associated Legendre functions. Alterman et al. [38] computed the short period free oscillations (acoustic modes) showing that the effect of rotation and ellipticity can be negligible for this type of oscillations. However, Smith [39] showed that the choice of the displacement field as a sum of toroidal and spheroidal components would give reasonable results for the Chandler wobble but for the wobble modes of the inner core, the truncations have had to be extended way beyond 3

to 4 terms [39]. Crossley [34] was able to extend the numerical computations of short period modes to high degrees of truncations for both the spheroidal $\mathbf{S}_n^m$ and toroidal $\mathbf{T}_n^m$ for different Earth models, thanks to the development of high speed computers. Besides the weakness of the traditional approach due to high truncation, it is not valid for the computations of many modes which are sensitive to the rotation and the ellipticity, especially the inertial modes and Slichter modes. Therefore, new alternatives were considered for the solution of the governing equations of the fluid core oscillations [37] .

The Subseismic Approximation (SSA) was developed by Smylie and Rochester (1981) to solve for the free oscillations of the Earth [40]. They were able to reduce the governing equations of the fluid core to only two scalar variables V_1, and χ. In this method, the contribution of the pressure perturbation $\frac{p_1}{\rho_0} << |\mathbf{g}_0 \cdot \mathbf{u}|$ is ignored in the entropy equation (1.12). Therefore, equations (1.11) and (1.12) become

$$\nabla \cdot (f\tilde{\mathbf{\Gamma}} \cdot \nabla\chi) = 0 \tag{1.19}$$

$$\frac{1}{4\pi G\rho_0}\nabla^2 V_1 = \frac{1}{B}\mathbf{C} \cdot \nabla\chi \tag{1.20}$$

where

$$\chi = \frac{p_1}{\rho_0} - V_1 \tag{1.21}$$

$$B = \frac{\alpha^2\omega^2}{\beta}(1-\mu^2) + g_0^2 - \mu^2(\widehat{\mathbf{k}} \cdot \mathbf{g}_0)^2 \tag{1.22}$$

$$\mathbf{C} = \mu^2\widehat{\mathbf{k}}\widehat{\mathbf{k}} \cdot \mathbf{g}_0 - \mathbf{g}_0 + i\mu\widehat{\mathbf{k}} \times \mathbf{g}_0 \tag{1.23}$$

$$\tilde{\mathbf{\Gamma}} = \tilde{\mathbf{1}} - \mu^2\widehat{\mathbf{k}}\widehat{\mathbf{k}} - \frac{\mathbf{C}^*\mathbf{C}}{B} + i\mu\widehat{\mathbf{k}} \times \tilde{\mathbf{1}} \tag{1.24}$$

$$\mu = \frac{2\Omega}{\omega} \tag{1.25}$$

where $\tilde{\mathbf{1}}$ is a unit tensor, and f the decompression term introduced by Friedlander [41]. In

this method, the Subseismic Wave Equation (SSWE) in (1.19) represents the major equation to be solved, and the other variables V_1, the field displacement $\mathbf{u}$, and the perturbation in density ρ_1 and the pressure p_1 are deduced from other relevant equations defined above.

The SSA was implemented by Rochester and Peng [42] to show frequency dependence of the load Love numbers at the ICB and Core Mantle Boundary (CMB). Love numbers are used to include the elasticity of the Earth's solid parts in the dynamical equations at the solid-liquid boundaries. They applied a variational principle to solve for the frequencies of the Slichter modes for a rotating, spherical and neutrally stratified Earth model. They showed that the SSA violates the conservation of the linear momentum near the CMB [25]. Furthermore, the Hermitian property of the matrix generated from the SSWE in equation (1.19) is violated [36, 42–44].

The shortcomings of the SSA, plus the inefficiency presented by the traditional approaches, motivated a search for different approaches for the solution of the governing equations of the fluid core dynamics. Wu and Rochester [43], proposed the Two Potential Description (TPD). The TPD represent a coupling pair of second order linear partial differential equations based on two scalar potential fields V_1 and χ [25]. This method bypasses the conventional representation of spheroidal and toroidal components of the field displacement $\mathbf{u}$ described earlier. The mathematical formulation of the TPD is

$$\nabla \cdot [\Gamma \cdot \nabla\chi + \omega^2(1-\mu^2)(\chi + V_1)\frac{\mathbf{C}^*}{B}] - \frac{\omega^2(1-\mu^2)}{\beta B}[\mathbf{C}\cdot\nabla\chi - \omega^2(1-\mu^2)(\chi+V_1)] = 0 \tag{1.26}$$

$$\frac{1}{4\pi G}\nabla^2 V_1 - \rho_0\frac{\mathbf{C}\cdot\nabla\chi}{B} - [\frac{1-\beta}{\alpha^2} + \frac{\omega^2(1-\mu^2)}{B}](\chi + V_1) = 0 \tag{1.27}$$

where B, $\mathbf{C}$ and $\tilde{\mathbf{\Gamma}}$ are defined above.

Figure 1.2: Fluid core (FC) stability parameter of PREM (Dziewonsky and Anderson, 1981)

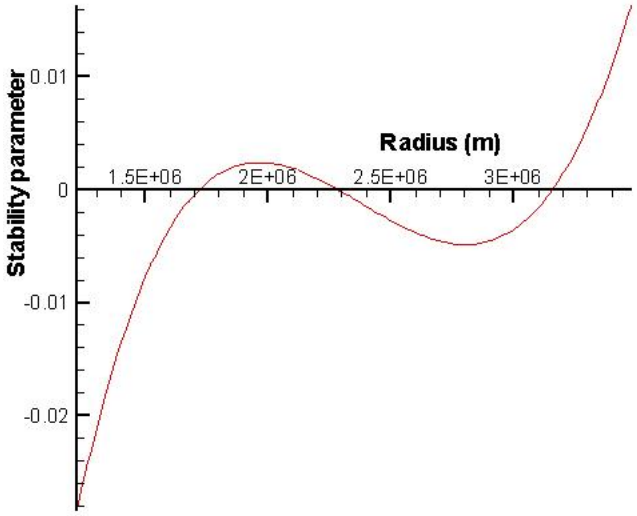

To discuss one of the limitations of the TPD, we show in figure 1.2 the stability parameter profile of the PREM model, and discuss the failure of this method due to its depedence on $1/\beta$ and also on $1/B$. It is obvious from figure 1.2 that there are three (03) singular points ($\beta = 0$). Therefore, the TPD becomes inadequate for such an Earth model [25]. Since the TPD equations have a $1/B$ dependence, they may also become unstable for some frequencies at which B tends to zero [25]. However, this method is useful for a neutrally stratified Earth model ($\beta = 0$). To remove the instability of the TPD equations, Peng [25] multiplied the equations (1.16) and (1.17) by the term $(\beta B)^2$ so that the governing equations become suitable for a numerical search for eigenperiods in a frequency range for which B may vanish somewhere in the liquid core.

To remedy on the above limitations, a new approach was develop by Seyed-Mahmoud

and Rochester (2006) [45], the three potential description (3PD), to study of the dynamics of the Earth's fluid core and rotating stars. Beside the linear character of the scalar representation in solving for the oscillations of the fluid core, the 3PD is a set of three equations describing the fluid core oscillations without any approximations [45,46]. We adopt the 3PD to solve for the dynamical equations of the Earth's core oscillations (see chapter 2).

1.3 Previous Work

We review some published work on the theoretical and observations of the Earth's core oscillations. Among the first to conduct studies of the inertial modes of the Earth were Hough [47] and Poincaré [48]. They found analytical solutions for the inertial modes of a spherical, incompressible, inviscid and homogenous core model. After a successful computation of the inertial modes, their theory was extended to treat more realistic cases.

There is a network of superconducting gravimeters installed around the globe in order to record the Earth's seismic activities for the identification of the Earth's oscillations such as the Slichter modes and other normal modes. Since the South Pole is seismically quiet, it is an ideal point for observing the translational oscillations of the inner core. Jackson and Slichter [30] proposed that if these modes were excited with an amplitude of up to 1 nanogal during the period of October 1970 to September 1971, they would have been recorded using the spring gravimeter (the gal or galileo, is a unit of acceleration used in the science of gravimetry, it is defined as 1 centimeter per second squared (1cm/s^2)) . At the lower limit of its detection, Crossley [34] showed that with PREM-like model, the Slichter mode excitations could produce a weak gravity signal of about 0.5 nanogal at the Earth's surface

for the Great Chilean Earthquake (1960).

The influence of the fluid core rotation on the Slichter mode was first studied by Busse [24]. He used a rotating Earth model with a rigid mantle, an incompressible, homogeneous and inviscid fluid core. He concluded that a change of 50% in the frequency of the Slichter modes could be seen if the action of the Coriolis force is taken into account, and that their rotational splitting was not symmetric. In addition to Busse's model, Crossley [49] and Smith [50] added to the rotation of the Earth the compressibility and the density stratification of the FC, with an elastic IC and mantle. They showed that these parameters added to Busse's model are important in the determination of the Slichter modes, and should therefore be considered for a realistic Earth model.

To account for the effects of the ellipticity, Smith [50] showed that the main contribution to the Slichter splitting is due to rotation, and the ellipticity affects the frequency of the central mode by 10%. Smith used Busse's Earth model [24], but with an elastic IC and a radially stratified FC. However, Smith's calculated period for the Slichter triplet was about 20% higher than those obtained by Busse's (7.653 to 6.397 h) [50]. Moreover, a perturbation theory was used by Dahlen and Sailor [51] to study the effects of the ellipticity and rotation on the free oscillations of the Earth. They include parameters of second order in rotation and ellipticity, and develop a convenient formula to evaluate the splitting coefficient, conclude that the frequencies of the Slichter modes for a spherical Earth are displaced only by about 0.1% when the elliptical figure of the Earth is considered.

The Slichter modes have been the subject of searches in data produced by the global network of gravimeters since a motion of the inner core would produce a small change in the

Earth's gravity field. After the Great Chilean Earthquake of May 22, 1960, a gravimeter peak near 86 min was tentatively identified by Slichter (1961) as originating from the inner core translational oscillations [29]. However, in 1992 research conducted by Smylie [52] using his theoretical prediction and analysis based on the recorded gravity data claimed the detection of the Slichter triplets. Shortly after Smylie's publication, authors such as Crossley [53], and Rochester and Peng [42], disputed Smylie's claims. They showed that it is not relevant to avoid the frequency-dependence of the load Love numbers, it is a parameter of great importance between the elastic IC and mantle to the liquid core, therefore, should be accounted. They concluded that it was unrealistic to use the static Love numbers for the rotational splitting [42].

Moreover, using geophysical processing tools to correct the noise in the data from seismic activities recorded across the worldwide gravimeter network, Jensen [54] and Hinderer [55] showed that the peaks identifed by Smylie [52] were not significant.

In 2000, Courtier et al., [56] using 294,106 hours of observations from station logs from different gravimeter across Europe, confirmed the presence of the Slichter triplets claimed by Smylie [52]. However, Rieutord [57] showed that the results of Courtier [56] do not agree with the observed Q factors (under-damped oscillations) of several recorded data, and could not be reproduced using a realistic dynamical Earth model. Rogister [58] using the PREM and 1066A Earth models, studied the splitting by rotation and ellipticity using normal mode theory and concluded that the ellipticity and the centrifugal force contibute 0.3% of the variation of the frequencies of the Slichter modes [58].

In addition, studies based on possible sources of excitation of the Slichter modes

have been conducted for a simple Earth model, composed of three layers (solid and deformable IC, FC and elastic mantle) by Marianne and Legros [59], and for a spherical, self-gravitating anelastic PREM-like Earth model by Rosat and Rogister [27]. They both concluded that the Slichter modes can best be excited by a pressure change at the core boundary at the time scale of half the Slichter periods [27], and for a considerable pressure of 100 Pa, the signal due to the Slichter triplet can be recorded at the Earth's surface using any sensitive superconducting gravimeters [59].

1.4 Thesis Scope

This thesis is divided into 5 chapters as follows: In chapter 2 we discuss the three potential descriptions (3PD). We then develop a Galerkin formulation which we apply to the 3PD to solve the dynamical equations. We expand the equations and use the orthogonality relation among spherical harmonics to implement the equation with respect to the radial component r. Next, we discuss the boundary conditions. In chapter 3, we discuss the Earth model and the parameters needed for this study, and also develop and expand the inner core equations of motion.

In chapter 4, the results of this work are discussed. We will first describe the procedure to solve for the frequencies of the inertial modes of the fluid core. The inertial modes of a spherical and rotating Earth with a solid inner core and neutrally stratified and compressible fluid core will be discussed and presented along with their eigenfunctions, and the discussion on the Slichter modes will follow. Finally, a summary and concluding remarks will be presented in chapter 5.

Chapter 2

GALERKIN FORMULATION OF THE 3PD AND BOUNDARY CONDITIONS

In this chapter, we briefly describe the 3PD in section 2.1, and summarize the method named after Boris Galerkin in section 2.2. The Galerkin method is widely used in the area of numerical analysis to convert continuous operator problems such as Partial Differential Equation (PDE) subject to boundary conditions to a discrete problem [60]. After a description of the Galerkin method, we will present the expansion of the 3PD in sections 2.3, 2.4 and 2.5. In section 2.6 we will implement the boundary conditions.

2.1 The Three Potential Description (3PD)

Constructed from the dilatation, the gravitational potential and the perturbation in pressure, the 3PD represent a set of 3 linearized equations in 3 scalar potentials describing the dynamics of a rotating, self gravitating, stratified, compressible and inviscid fluid body [45].

To construct the 3PD, the reference state is considered one of hydrostatic equilibrium, rotating with the rate $\mathbf{\Omega}$ about the unit vector fixed in the inertial space $\widehat{\mathbf{e}}_3$. The motion of the fluid is considered as oscillatory. Based on the conservation of laws described in chapter 1 for the mass, momentum, gravitational flux, and entropy in equations (1.6)-(1.9) respectively, and also replacing the time dependence of these equations with $e^{i\omega t}$. With the choice of 3 scalars potentials defined as $\chi = \frac{p_1}{\rho_0}$, $\zeta = \nabla \cdot \mathbf{u}$ and V_1. After several mathematical operations on the equations (1.6)-(1.9). By using the dimensionless terms are $\chi^{'} = \frac{\chi}{4\Omega^2 R^2}$, $V_1^{'} = \frac{V_1}{4\Omega^2 R^2}$, the local wave speed $\alpha = \frac{\alpha^{'}}{2\Omega R}$, the Poincare tensor $\tilde{\mathbf{\Gamma}}^{'}_P = \frac{\widehat{\mathbf{\Gamma}}_P}{4\Omega^2}$, the modal frequency $\sigma = \frac{\omega}{2\Omega}$, the gravity $\mathbf{g}_0^{'} = \frac{\mathbf{g}_0}{4R\Omega^2}$, and the dimensionless constant of gravitation $G' = \frac{G\rho_0}{4\Omega^2}$. Where R is the radius of the Earth, Ω the Earth's rotation rate, the notation $(^{'})$ is used to represent the dimensionless terms. We write the dimensionless equations of 3PD (see Seyed-Mahmoud and Rochester, 2006 [45])

$$\nabla \cdot \left[\tilde{\mathbf{\Gamma}}_p \cdot \nabla(\chi - V_1) - \beta \mathbf{C}^* \zeta\right] - \sigma^2(\sigma^2 - 1)\zeta = 0 \tag{2.1}$$

$$\nabla^2 V_1 - 4\pi G\left(\beta\zeta - \frac{1-\beta}{\alpha^2}\chi\right) = 0 \tag{2.2}$$

$$\mathbf{C} \cdot \nabla(\chi - V_1) - \sigma^2(\sigma^2 - 1)\chi - B\zeta = 0 \tag{2.3}$$

where

$$\tilde{\mathbf{\Gamma}}_P = \sigma^2\tilde{\mathbf{1}} - \widehat{e}_3\widehat{e}_3 + i\sigma\widehat{e}_3 \times \tilde{\mathbf{1}}, \tag{2.4}$$

$$\mathbf{C} = -\sigma^2\mathbf{g}_0 + \widehat{e}_3 \cdot \mathbf{g}_0\widehat{e}_3 + i\sigma\widehat{e}_3 \times \mathbf{g}_0, \tag{2.5}$$

$$B = \alpha^2\sigma^2(\sigma^2 - 1) + \beta\left[\sigma^2\mathbf{g}_0^2 - (\widehat{e}_3 \cdot \mathbf{g}_0)^2\right], \tag{2.6}$$

where $\tilde{\mathbf{1}}$ is the unit dyadic, and for convenience we have dropped the $(')$ notation from all terms. Equations (2.1), (2.2), and (2.3) are known as the 3PD. They are composed of two second and one first order differential equations describing the dynamics of an oscillating fluid body via 3 scalars χ, ζ, V_1 without approximations [37, 45].

The boundary conditions require that at all boundaries the following conditions are met:

- continuity of the normal component of the displacement, $\widehat{\mathbf{n}} \cdot \mathbf{u}$,

- continuity of the normal component of the gravitational flux, $\widehat{\mathbf{n}} \cdot (\nabla V_1 - 4\pi G\rho_0\mathbf{u})$,

- continuity of the normal component of the stress tensor, $\widehat{\mathbf{n}} \cdot \tilde{\tau}$,

- continuity of the perturbation in the gravitational potential, V_1,

where $\widehat{\mathbf{n}}$, and $\tilde{\tau} = -(p_1 + \mathbf{u} \cdot \nabla p_0)\tilde{\mathbf{1}}$ are the unit normal vector to the boundary surface, and the additional stress developed by the deformation superimposed on the equilibrium pressure.

2.2 The Galerkin Method

The Galerkin method is a tool to approximate the solution of an operator equation in the form of a linear combination of the elements of a linear independent system [61]. Following Seyed-Mahmoud's work [37], and suppose we have a set of functions $\chi = (\chi_1, \chi_2, ..., \chi_n)$ which satisfies, in a region V, the set of simultaneous PDEs

$$\sum_{j=1}^{N} L_{ij}\chi_j = 0, \ (i = 1, ...N) \tag{2.7}$$

where L_{ij} are linear partial differential operator. Suppose also that for a linear operator B_{ij} which satified a set of boundary conditions S, such that

$$\sum_{j=1}^{M} B_{ij}\chi_j = 0, \ (i = 1, ...N) \tag{2.8}$$

Using a set of basis functions f_k, $k = 1, ..., L$, introduce trial functions $\chi_j = \sum_{k=1}^{L} C_{jk}f_k$, for every $j = 1, ..., N$, which need not a priori satisfy the boundary conditions. The Galerkin formulation requires that

$$\sum_{j=1}^{N}\sum_{k=1}^{L}\int_V f^*_{k'}L_{ij}C_{jk}f_k dV = 0, \ (k' = 1, ...L) \tag{2.9}$$

where $(^*)$ denote the complex conjugate of f_k. The problem in equation (2.9) is changed into a matrix formulation as

$$\sum_{j=1}^{N}\sum_{k=1}^{L}\int_V H_{k'ijk}C_{jk} = 0, \tag{2.10}$$

where $H_{k'ijk} = \int_V f^*_{k'}L_{ij}f_k$. In general the trial functions do not a priori satisfy the boundary conditions. A set of basis functions equal in number to the basis functions defined in the trial functions is used to reconstruct in addition equation (2.9) as

$$\sum_{j=1}^{N}\sum_{k=1}^{L}\left[\int_V f^*_{k'}L_{ij}C_{jk}f_k dV + \int_S g^*_{k'}B_{ij}C_{jk}f_k dS\right] = 0, \tag{2.11}$$

Therefore, the Galerkin formulation is then given by

$$F_{k'ijk} = H_{k'ijk} + \int_S g^*_{k'} B_{ij} f_k dS \tag{2.12}$$

where $g_{k'}$ are the weighted functions. The surface integral can possibly be removed by implementing the divergence theorem, which arises by the conversion of the volume integral to a surface one. When this happens with a proper choice of weighted functions, the boundary conditions are considered natural.

In this study, a conventional approach to solving the 3PD is to consider spherical harmonics for the three scalars potential V_1, χ, ζ, and apply the Galerkin method, which reduces the set of differential equations into a system of matrices. Once the matrix is generated the solution can be estimated by any numerical method [25,37,60–62]. For further calculations we choose the trial functions as

$$V_1 = \sum_{n=|m|}^{N} \sum_{l=1}^{L} E_{[L(n)+l]} f_l(x) Y_n^m(\theta, \phi), \tag{2.13}$$

$$\chi = \sum_{n=|m|}^{N} \sum_{l=1}^{L} E_{[L(N+n)+l]} f_l(x) Y_n^m(\theta, \phi), \tag{2.14}$$

$$\zeta = \sum_{n=|m|}^{N} \sum_{l=1}^{L} E_{[L(2N+n)+l]} f_l(x) Y_n^m(\theta, \phi) \tag{2.15}$$

where $f_l(x)$ is a function of the dimensionless radius $x = \frac{r}{R}$ and can be any functions, where r is the varying radius of the Earth, and R the mean Earth radius. As one of the objectives of this study is to test the convergence of the results, the completeness requirement for varying N, or L is an advantage of using the Galerkin formulation, therefore in this study, we consider the Legendre functions for $f_l(x)$, since we can vary both $N, L \to \infty$, or any other functions which can be used to test the convergence of the results [63]. The argument

x of f_l is defined in equation (2.16) below

$$x = \frac{2r}{b-a} - \frac{b+a}{b-a} \tag{2.16}$$

where a and b are the dimensionless inner and outer radii of the spherical shell, and $a \leq r \leq b$.

2.3 Galerkin Formulation of the Poisson Equation

The Galerkin formulation of Poisson's equation can be written as

$$\begin{aligned} &\int_V f_{l'}(x) Y_q^{m*} \nabla^2 V_1 dV - 4\pi G \int_V f_{l'}(x) Y_q^{m*} \left(\beta\zeta - \frac{1-\beta}{\alpha^2}\chi\right) dV \\ &+ \int_{ICB+CMB} \psi_{l'}^*(x)[\widehat{\mathbf{n}} \cdot (\nabla V_1 - 4\pi G\rho_0 \mathbf{u}) - \widehat{\mathbf{n}} \cdot (\nabla V_1^{'} - 4\pi G\rho_{IC}\mathbf{u}_{IC})]dS = 0, \end{aligned} \tag{2.17}$$

where $l' = 1, ..., L$ and ρ_{IC}, ρ_0, $\mathbf{u}$, $\mathbf{u}_{IC}$, G, V_1 and $V_1^{'}$ are the density of the inner core, and the density of the fluid core near the ICB, the displacement of the fluid near the ICB, the inner core displacement, the dimensionless gravitational constant, the perturbation in gravitational potential for the fluid near the ICB, and for the inner core respectively. The surface integral terms added to the Poisson equation are used to consider the natural character of the boundary conditions. Applying the divergence theorem on the first term $f_{l'}(x) Y_q^{m*} \nabla^2 V_1$, with a proper choice of the weighted functions $\psi_{l'}^*(x) = -f_{l'}(x) Y_q^{m*}$, and with the implementation of the boundary conditions $\widehat{\mathbf{n}} \cdot \mathbf{u} = \widehat{\mathbf{n}} \cdot \mathbf{u}_{IC}$, we can rewrite equation (2.17) as

$$\begin{aligned} &\int_V \nabla \left[f_{l'}(x) Y_q^{m*}\right] \cdot \nabla V_1 dV + 4\pi G \int_V f_{l'}(x) Y_q^m \left(\beta\zeta - \frac{1-\beta}{\alpha^2}\chi\right) dV \\ &- \int_{FC+LC} f_{l'}(x) Y_n^{m*}[4\pi G(\rho_0 - \rho_{IC})\widehat{\mathbf{n}} \cdot \mathbf{u}_{IC} + \widehat{\mathbf{n}} \cdot \nabla V_1^{'}]dS = 0 \end{aligned} \tag{2.18}$$

For convenience, we write

$$PE1 = \int_V \nabla \left[f_{l'}(x) Y_q^{m*} \right] \cdot \nabla V_1 dV \tag{2.19}$$

$$PE2 = 4\pi G \int_V f_{l'}(x) Y_q^m \left(\beta\zeta - \frac{1-\beta}{\alpha^2}\chi \right) dV \tag{2.20}$$

$$PE3 = \int_{FC+LC} f_{l'}(x) Y_n^{m*} [4\pi G(\rho_0 - \rho_{IC}) \widehat{\mathbf{n}} \cdot \mathbf{u}_{IC} + \widehat{\mathbf{n}} \cdot \nabla V_1^{'}] dS \tag{2.21}$$

The surface integral in the PE3 term of equation (2.21) will be developed later using the implementation of the boundary conditions. By using the spherical harmonic representation of the trial functions, following the gradient operations shown in apendix A.1, we can operate $\nabla \left[f_{l'}(x) Y_q^{m*} \right] \cdot \nabla V_1$ and then rewrite PE1 as

$$\begin{aligned} PE1 = \sum_{n=|m|}^{N} \sum_{l=1}^{L} E_{[L(n)+l]} \int_V \left[\frac{df_l(x)}{dx} \frac{df_{l'}(x)}{dx} P_q^m P_n^m + \frac{1}{x^2} f_{l'}(x) f_l(x) \frac{dP_q^m}{d\theta} \frac{dP_n^m}{d\theta} \right. \\ \left. + \frac{m^2}{x^2 sin^2\theta} f_{l'}(x) f_l(x) P_q^m P_n^m \right] dV \end{aligned} \tag{2.22}$$

Substituting $dV = x^2 \sin\theta \; d\theta \; d\phi \; dx$ and knowing that

$$\int_0^\pi \frac{dP_q^m}{d\theta} \frac{dP_n^m}{d\theta} sin\theta d\theta = \int_0^\pi \left[n(n+1) - \frac{m^2}{sin^2\theta} \right] P_q^m P_n^m \sin\theta d\theta \tag{2.23}$$

we write equation (2.22) as

$$PE1 = \sum_{l=1}^{L} E_{[L(q)+l]} \int \left[x^2 \frac{df_l(x)}{dx} \frac{df_{l'}(x)}{dx} + q(q+1) f_{l'}(x) f_l(x) \right] dx \int P_n^m P_q^m \sin\theta d\theta \tag{2.24}$$

The development of PE2 in equation (2.20) is given by

$$\begin{aligned} PE2 = 4\pi G \sum_{l=1}^{L} \left[E_{[L(2N+q)+l]} \int \beta x^2 f_{l'}(x) f_l(x) dx \right. \\ \left. - E_{[L(N+q)+l]} \int \frac{1-\beta}{\alpha^2} x^2 f_{l'}(x) f_l(x) dx \int P_n^m P_q^m \sin\theta d\theta \right] \end{aligned} \tag{2.25}$$

We know that the orthogonality relation of the associated Legendre polynomials is given by

$$\int \int Y_q^{m*} Y_n^m \sin\theta d\theta d\phi = 2\pi \int P_q^m P_n^m \sin\theta d\theta = 2\pi \frac{2(n+m)!}{(2n+1)(n-m)!} \delta_n^q \tag{2.26}$$

where δ_n^q is the Kronecker delta, which is zero for $n \neq q$ and 1 only for $n = q$. However, we will just drop the constant in front of the orthogonality relation since the Poisson equation (2.17) equal to zero. Therefore, we finally rewrite the Galerkin formulation of Poisson's equation as:

$$\begin{aligned} &- PE3 + \sum_{l=1}^{L} \int \left[E_{[L(q)+l]} \left(x^2 \frac{df_l(x)}{dx} \frac{df_{l'}(x)}{dx} + q(q+1) f_{l'}(x) f_l(x) \right) \right. \\ &\left. + 4\pi G \left(E_{[L(2N+q)+l]} \beta x^2 f_{l'}(x) f_l(x) - E_{[L(N+q)+l]} \frac{1-\beta}{\alpha^2} x^2 f_{l'}(x) f_l(x) \right) \right] dx = 0, \end{aligned} \tag{2.27}$$

where the term PE3 will later be completed after the implementation of the boundary conditions in section 2.6. Note that equation (2.27) is a function of x only, that is we have integrated the Poisson equation analytically with respect to θ and ϕ.

2.4 Galerkin Formulation of the Momentum Equation

The Galerkin formulation of the momentun equation can be written as

$$\begin{aligned} &\int_V f_{l'}(x) Y_q^{m*} \left[\nabla \cdot \left(\tilde{\mathbf{\Gamma}}_p \cdot \nabla(\chi - V_1) - \beta \mathbf{C}^* \zeta \right) - \sigma^2(\sigma^2 - 1)\zeta \right] dV \\ &+ \int_{ICB+LC} \psi_{l'}(x) \widehat{\mathbf{n}} \cdot (\mathbf{u} - \mathbf{u}_{IC}) dS = 0, \end{aligned} \tag{2.28}$$

where $l' = 1, ..., L$ and Y_q^{m*} the complex conjugate spherical harmonics of order m, and degree q, $\mathbf{u}$, and $\mathbf{u}_{IC}$ are the displacement of the fluid core and inner core respectively. Applying the divergence theorem, we can write

$$\begin{aligned} &\int_S \widehat{\mathbf{n}} \cdot \left[f_{l'}(x) Y_q^{m*} \left(\tilde{\mathbf{\Gamma}}_p \cdot \nabla(\chi - V_1) - \beta \mathbf{C}^* \zeta \right) \right] dS - \sigma^2(\sigma^2 - 1) \int_V f_{l'}(x) Y_q^{m*} \zeta dV \\ &- \int_V \nabla(f_{l'}(x) Y_q^{m*}) \cdot \left(\tilde{\mathbf{\Gamma}}_p \cdot \nabla(\chi - V_1) - \beta \mathbf{C}^* \zeta \right) dV \\ &+ \int_{ICB+LC} \psi_{l'}(x) \widehat{\mathbf{n}} \cdot (\mathbf{u} - \mathbf{u}_{IC}) dS = 0. \end{aligned} \tag{2.29}$$

We know from the implementation of the 3PD in equation (21) of Seyed-Mahmoud and Rochester's work [45] that

$$\tilde{\mathbf{\Gamma}}_p \cdot \nabla(\chi - V_1) - \beta \mathbf{C}^* \zeta = \sigma^2(\sigma^2 - 1)\mathbf{u} \tag{2.30}$$

therefore, with a proper choice of $\psi^*_{l'}(x) = -f_{l'}(x)Y^{m*}_q$, and with the substitution of the boundary condition $\widehat{\mathbf{n}} \cdot \mathbf{u} = \widehat{\mathbf{n}} \cdot \mathbf{u}_{IC}$ at the inner core boundary, and at the core mantle boundary $\widehat{\mathbf{n}} \cdot \mathbf{u} = 0$, we then rewrite equation (2.29) as

$$\begin{aligned} &\sigma^2(\sigma^2-1)\int_S f_{l'}(x)Y^{m*}_q \widehat{n} \cdot \mathbf{u}_{IC} dS - \sigma^2(\sigma^2-1)\int_V f_{l'}(x)Y^{m*}_q \zeta dV \\ &- \int_V \nabla(f_{l'}(x)Y^{m*}_q) \cdot \left[\tilde{\mathbf{\Gamma}}_p \cdot \nabla(\chi - V_1)\right] dV + \beta \int_V \nabla(f_{l'}(x)Y^{m*}_q) \cdot \mathbf{C}^* \zeta dV = 0 \end{aligned} \tag{2.31}$$

For a clear expansion, we write

$$ME1 = \int_S f_{l'}(x)Y^{m*}_q \widehat{\mathbf{n}} \cdot \mathbf{u}_{IC} dS \tag{2.32}$$

$$ME2 = \int_V f_{l'}(x)Y^{m*}_q \zeta dV \tag{2.33}$$

$$ME3 = \int_V \nabla(f_{l'}(x)Y^{m*}_q) \cdot \left[\tilde{\mathbf{\Gamma}}_p \cdot \nabla(\chi - V_1)\right] dV \tag{2.34}$$

$$ME4 = \int_V \nabla(f_{l'}(x)Y^{m*}_q) \cdot \mathbf{C}^* \zeta dV \tag{2.35}$$

The term ME1 will be expanded in the next section dealing with the boundary conditions. We now expand equation (2.31) term by term, starting with the third term ME3. Therefore, with the substitution of the Poincaré tensor we write

$$\begin{aligned} ME3 = \int \big\{ &\sigma^2 \nabla(f_{l'}(x)Y^{m*}_q) \cdot \nabla(\chi - V_1) - [\nabla(f_{l'}(x)Y^{m*}_q) \cdot \widehat{\mathbf{e}}_3][\widehat{\mathbf{e}}_3 \cdot \nabla(\chi - V_1)] \\ &+ i\sigma \nabla(f_{l'}(x)Y^{m*}_q) \cdot (\widehat{\mathbf{e}}_3 \times \tilde{\mathbf{1}}) \cdot \nabla(\chi - V_1) \big\} dV \end{aligned} \tag{2.36}$$

In a spherical coordinate system, $\tilde{\mathbf{1}} = \widehat{\mathbf{rr}} + \widehat{\theta\theta} + \widehat{\phi\phi}$, and $\widehat{e}_3 = \widehat{\mathbf{r}}cos\theta - \widehat{\theta}sin\theta$. By using the gradient operations shown in appendix A.1, we get

$$\int \nabla(f_{l'}(x)Y_q^{m*}) \cdot (\widehat{e}_3 \times \widehat{1}) \cdot \nabla(\chi - V_1)dV = -im \sum_{n=|m|}^{N} \sum_{l=1}^{L} (E_{[L(N+n)+l]} - E_{[L(n)+l]}) \times$$
$$\int \int \left[\frac{\cos\theta}{x^2 \sin\theta} f_{l'}(x) f_l(x) P_q^m \frac{dP_n^m}{d\theta} + \frac{\cos\theta}{x^2 \sin\theta} f_{l'}(x) f_l(x) P_n^m \frac{dP_q^m}{d\theta} + \frac{1}{x} f_{l'}(x) \frac{df_l(x)}{dx} P_n^m P_q^m \right.$$
$$\left. + \frac{1}{x} f_l(x) \frac{df_{l'}(x)}{dx} P_n^m P_q^m \right] \sin\theta d\theta d\phi. \tag{2.37}$$

We use the identity [37]

$$\int \frac{\cos\theta}{\sin\theta} \left(P_q^m \frac{dP_n^m}{d\theta} + P_n^m \frac{dP_q^m}{d\theta} \right) \sin\theta d\theta = \int P_n^m P_q^m \sin\theta d\theta. \tag{2.38}$$

Substituting equation (2.38) into equation (2.37), we write

$$\int \nabla(f_{l'}(x)Y_q^{m*}) \cdot (\widehat{e}_3 \times \widehat{\mathbf{1}}) \cdot \nabla(\chi - V_1)dV = -im \sum_{n=|m|}^{N} \sum_{l=1}^{L} (E_{[L(N+n)+l]} - E_{[L(n)+l]}) \times$$
$$\int \left[f_{l'}(x) f_l(x) + x f_{l'}(x) \frac{df_l(x)}{dx} + x f_l(x) \frac{df_{l'}(x)}{dx} \right] dx \int P_n^m P_q^m \sin\theta d\theta \int d\phi, \tag{2.39}$$

However, following the transformations in the above section for the term PE1 in equation (2.19), we get

$$\int \nabla(f_{l'}(x)Y_q^{m*}) \cdot \nabla(\chi - V_1)dV = \sum_{n=|m|}^{N} \sum_{l=1}^{L} (E_{[L(N+n)+l]} - E_{[L(n)+l]}) \times$$
$$\int \left[x^2 \frac{df_{l'}(x)}{dx} \frac{df_l(x)}{dx} + n(n+1) f_{l'}(x) f_l(x) \right] dx \int d\phi \int P_n^m P_q^m \sin\theta d\theta, \tag{2.40}$$

Following the above scheme of calculations and using the identities of associated Legendre's polynomials below [37]

$$\int P_2^1 \frac{dP_q^m}{d\theta} P_n^m \sin\theta d\theta = \int \left(6P_2 P_n^m - P_2^1 \frac{dP_n^m}{d\theta} \right) P_q^m \sin\theta d\theta \tag{2.41}$$

$$\int sin^2\theta \frac{dP_q^m}{d\theta}\frac{dP_n^m}{d\theta}\sin\theta d\theta = \int \left[\frac{2}{3}n(n+1) - m^2 - \frac{2}{3}n(n+1)P_2\right] P_n^m P_q^m + \frac{2}{3}\int P_2^1 P_q^m \frac{dP_n^m}{d\theta}\sin\theta d\theta, \tag{2.42}$$

we rewrite the second term of ME3 in equation (2.36) as

$$\begin{aligned}\int [\nabla(f_{l'}(x)Y_q^{m*})\cdot\widehat{\mathbf{e}}_3][\widehat{\mathbf{e}}_3\cdot\nabla(\chi - V_1)]dV = \sum_{l=1}^{L}(E_{[L(N+n)+l]} - E_{[L(n)+l]})\times \\ \int\int\int \left(\left[(\frac{2}{3}n(n+1) - m^2)f_{l'}(x)f_l(x) + \frac{1}{3}x^2\frac{df_l(x)}{dx}\frac{df_{l'}(x)}{dx}\right]P_n^m P_q^m \right. \\ + \left[\frac{2}{3}x^2\frac{df_l(x)}{dx}\frac{df_{l'}(x)}{dx} + 2xf_{l'}(x)\frac{df_l(x)}{dx} - \frac{2}{3}n(n+1)f_{l'}(x)f_l(x)\right]P_2 P_n^m P_q^m \\ \left. + \left[\frac{2}{3}f_{l'}(x)f_l(x) - \frac{1}{3}xf_{l'}(x)\frac{df_l(x)}{dx} + \frac{1}{3}xf_l(x)\frac{df_{l'}(x)}{dx}\right]P_2^1 P_q^m \frac{dP_n^m}{d\theta}\right)\sin\theta dx d\theta d\phi\end{aligned} \tag{2.43}$$

Since the summation is over all n, we use the following two identities

$$P_2 P_n^m = A_n^m P_{n-2}^m + B_n^m P_n^m + C_n^m P_{n+2}^m \tag{2.44}$$

$$P_2^1 \frac{dP_n^m}{d\theta} = 2(n+1)A_n^m P_{n-2}^m + 3B_n^m P_n^m - 2nC_n^m P_{n+2}^m \tag{2.45}$$

where

$$A_n^m = \frac{3(n+m)(n+m-1)}{2(2n+1)(2n-1)}$$

$$B_n^m = \frac{n(n+1) - 3m^2}{(2n+3)(2n-1)}$$

$$C_n^m = \frac{3(n+2-m)(n+1-m)}{2(2n+3)(2n+1)}$$

By expanding the chain with P_2 and P_2^1, since the summation is all over n, equations (2.44) and (2.45) are transformed as a function of P_n^m, by interchanging n from the constant A_n^m, B_n^m and C_n^m with those attached to the associated Legendre polynomial, and vice versa.

Substituting the orthogonality relation of associated Legendre polynomials, also we know that the Kronecker delta involved while integrating with respect to θ only survives for $n = q$. We therefore, rearrange terms with respect to $E_{[L(N+q+2)+l]}$, $E_{[L(N+q)+l]}$, and $E_{[L(N+q-2)+l]}$, and finally rewrite ME3 as:

$$
\begin{aligned}
ME3 = \sum_{l=1}^{L} \int \Bigg\{ \Bigg[& \sigma^2 \left(x^2 \frac{df_l(x)}{dx}\frac{df_{l'}(x)}{dx} + q(q+1) f_{l'}(x) f_l(x) \right) - \left(\frac{2}{3} q(q+1) - m^2\right) f_{l'}(x) f_l(x) \\
& + m\sigma \left(f_{l'}(x) f_l(x) + x f_{l'}(x) \frac{df_l(x)}{dx} + x f_l(x) \frac{df_{l'}(x)}{dx} \right) - \frac{x^2}{3} \frac{df_l(x)}{dx}\frac{df_{l'}(x)}{dx} \\
& - \left(\frac{2x^2}{3} \frac{df_l(x)}{dx}\frac{df_{l'}(x)}{dx} + 2x f_{l'}(x) \frac{df_l(x)}{dx} - \frac{2}{3} q(q+1) f_{l'}(x) f_l(x) \right) B_q^m \\
& - \left(2 f_{l'}(x) f_l(x) - x f_{l'}(x) \frac{df_l(x)}{dx} + x f_l(x) \frac{df_{l'}(x)}{dx} \right) B_q^m \Bigg] \left(E_{[L(N+q)+l]} - E_{[L(q)+l]} \right) \\
& - A_{q+2}^m \Bigg[\left(\frac{2x^2}{3} \frac{df_l(x)}{dx}\frac{df_{l'}(x)}{dx} + 2x f_{l'}(x) \frac{df_l(x)}{dx} - \frac{2}{3}(q+2)(q+3) f_{l'}(x) f_l(x) \right) \\
& + 2(q+3) \left(\frac{2}{3} f_{l'}(x) f_l(x) - \frac{x}{3} f_{l'}(x) \frac{df_l(x)}{dx} + \frac{x}{3} f_l(x) \frac{df_{l'}(x)}{dx} \right) \Bigg] \left(E_{[L(N+q+2)+l]} - E_{[L(q+2)+l]} \right) \\
& - C_{q-2}^m \Bigg[\left(\frac{2x^2}{3} \frac{df_l(x)}{dx}\frac{df_{l'}(x)}{dx} + 2x f_{l'}(x) \frac{df_l(x)}{dx} - \frac{2}{3}(q-2)(q-1) f_{l'}(x) f_l(x) \right) \\
& - 2(q-2) \left(\frac{2}{3} f_{l'}(x) f_l(x) - \frac{x}{3} f_{l'}(x) \frac{df_l(x)}{dx} + \frac{x}{3} f_l(x) \frac{df_{l'}(x)}{dx} \right) \Bigg] \left(E_{[L(N+q-2)+l]} - E_{[L(q-2)+l]} \right) \Bigg\} dx
\end{aligned}
\tag{2.46}
$$

To develop the term ME4 of equation (2.31), we need to define in the spherical coordinate system the gravity as $\mathbf{g}_0 = -g_0 \widehat{\mathbf{r}}$, where g_0 is evaluated in appendix A.2. We now first expand $\mathbf{C}^* \zeta$ as

$$
\mathbf{C}^* \zeta = g_0 \sum_{n=|m|}^{N} \sum_{l=1}^{L} \left[(\sigma^2 - \cos^2\theta) \widehat{\mathbf{r}} + (\cos\theta \sin\theta + \sigma^2) \widehat{\theta} - i\sigma \sin\theta \widehat{\phi} \right] E_{[L(2N+n)+l]} f_l(x) Y_n^m
\tag{2.47}
$$

Therefore, we write ME4 as

$$\begin{aligned} ME4 = \sum_{n=|m|}^{N}\sum_{l=1}^{L}\int\int\int \Big[& (\sigma^2 - \cos^2\theta)x^2 f_l(x)\frac{df_{l'}(x)}{dx}P_q^m P_n^m \\ & +(\cos\theta\sin\theta + \sigma^2)x f_{l'}(x) f_l(x) P_n^m \frac{dP_q^m}{d\theta} \\ & -m\sigma x f_{l'}(x) f_l(x) P_q^m P_n^m \Big] E_{[L(2N+n)+l]} dx \sin\theta d\theta d\phi \end{aligned} \tag{2.48}$$

We know that $\cos^2\theta = \frac{2P_2}{3} + \frac{1}{3}$ and $P_2^1 = -3\cos\theta\sin\theta$, and substituting into equation (2.48), we write ME4 as

$$\begin{aligned} ME4 = g_0 \sum_{n=|m|}^{N}\sum_{l=1}^{L}\Bigg\{ \Bigg[& \left(-\frac{2}{3}x^2 f_l(x)\frac{df_{l'}(x)}{dx} + 2x f_{l'}(x) f_l(x)\right) P_2 \\ & -\frac{m\sigma}{x} f_{l'}(x) f_l(x) - \left(\frac{1}{3} - \sigma^2\right) f_l(x)\frac{df_{l'}(x)}{dx}\Bigg] P_q^m P_n^m \\ & -\frac{1}{3}x f_{l'}(x) f_l(x) P_2^1 P_q^m \frac{dP_n^m}{d\theta}\Bigg\} E_{[L(2N+n)+l]}, \end{aligned} \tag{2.49}$$

Using the identity in equations (2.44) and (2.45) and substituting the orthogonality relation of the associated Legendre polynomials, which only survive for $n = q$, we therefore, rearrange terms with respect to $E_{[L(2N+q+2)+l]}$, $E_{[L(2N+q)+l]}$, and $E_{[L(2N+q-2)+l]}$, and finally rewrite ME4 as:

$$\begin{aligned} ME4 = g_0 \sum_{l=1}^{L}\int\Bigg\{ \Bigg[& -m\sigma x f_{l'}(x) f_l(x) - \left(\frac{1}{3} - \sigma^2\right) x^2 f_l(x)\frac{df_{l'}(x)}{dx} \\ & -x f_{l'}(x) f_l(x) B_q^m + \left(2x f_{l'}(x) f_l(x) - \frac{2x^2}{3} f_l(x)\frac{df_{l'}(x)}{dx}\right) B_q^m \Bigg] E_{[L(2N+q)+l]} \\ & +A_{q+2}^m \left(2x f_{l'}(x) f_l(x) - \frac{2x^2}{3} f_l(x)\frac{df_{l'}(x)}{dx} - \frac{2(q+3)}{3} x f_{l'}(x) f_l(x)\right) E_{[L(2N+q+2)+l]} \\ & +C_{q-2}^m \left(2x f_{l'}(x) f_l(x) - \frac{2x^2}{3} f_l(x)\frac{df_{l'}(x)}{dx} + \frac{2(q-2)}{3} x f_{l'}(x) f_l(x)\right) E_{[L(2N+q-2)+l]}\Bigg\} dx. \end{aligned} \tag{2.50}$$

Next, the term ME2 is therefore written as

$$ME2 = \sum_{l=1}^{L}\int x^2 f_{l'}(x) f_l(x) E_{[L(2N+q)+l]}. \tag{2.51}$$

We keep the first term ME1 as it is defined in equation (2.32), and will discuss it later in section 2.6. Therefore, by adding ME2, ME3 and ME4, the Galerkin formulation of the momentum equation is given by

$$-\sigma^2(\sigma^2-1)ME1+\sigma^2(\sigma^2-1)ME2+ME3-\beta ME4=0 \tag{2.52}$$

2.5 Galerkin Formulation of the Entropy Equation

The Galerkin formulation of the entropy equation can be written as

$$\begin{aligned}&\int_V f_{l'}(x)Y_q^{m*}\left[\mathbf{C}\cdot\nabla\left(\chi-V_1\right)\right]dV-\sigma^2\left(\sigma^2-1\right)\int_V f_{l'}(x)Y_q^{m*}\chi dV\\&-\int_V f_{l'}(x)Y_q^{m*}B\zeta dV=0\end{aligned} \tag{2.53}$$

For simplicity of the calculations, we use

$$\begin{aligned}EE1&=\int_V f_{l'}(x)Y_q^{m*}\left[\mathbf{C}\cdot\nabla\left(\chi-V_1\right)\right]dV\\EE2&=\int_V f_{l'}(x)Y_q^{m*}\chi dV\\EE3&=\int_V f_{l'}(x)Y_q^{m*}B\zeta dV\end{aligned} \tag{2.54}$$

From the expansion of $\mathbf{C}$ in the spherical coordinate system in equation (2.47), we write

$$\mathbf{C}=g_0\left[(\sigma^2-\cos^2\theta)\widehat{r}+\sin\theta\cos\theta\widehat{\theta}-i\sigma\sin\theta\widehat{\phi}\right],$$

we therefore, operate $\mathbf{C}\cdot\nabla\left(\chi-V_1\right)$ as

$$\begin{aligned}\mathbf{C}\cdot\nabla\left(\chi-V_1\right)=g_0\sum_{n=|m|}^{N}\sum_{l=1}^{L}\left(E_{[L(N+n)+l]}-E_{[L(n)+l]}\right)\Bigg[&(\sigma^2-\cos^2\theta)\frac{df_l(x)}{dx}Y_n^m\\&+\sin\theta\cos\theta\frac{1}{x}\frac{dP_n^m}{d\theta}f_l(x)e^{im\phi}+\frac{m\sigma}{x}f_l(x)Y_n^m\Bigg]\end{aligned}$$

Integrating with respect to θ, and using the recurrence relation in equations (2.44) and (2.45), and also using the orthogonality relation in equation (2.26), we rewrite EE1 as

$$\begin{aligned} EE1 = g_0 \sum_{l=1}^{L} \int \Bigg\{ \Bigg[& (\sigma^2 - \frac{1}{3}) x^2 f_{l'}(x) \frac{df_l(x)}{dx} \\ & + m\sigma f_{l'}(x) f_l(x) - \frac{2}{3} x^2 f_{l'}(x) \frac{df_l(x)}{dx} B_q^m - x f_{l'}(x) f_l(x) B_q^m \Bigg] \left(E_{[L(N+q)+l]} - E_{[L(q)+l]} \right) \\ & - A_{q+2}^m \left[\frac{2}{3} x^2 f_{l'}(x) \frac{df_l(x)}{dx} + \frac{2(q+3)}{3} x f_{l'}(x) f_l(x) \right] \left(E_{[L(N+q+2)+l]} - E_{[L(q+2)+l]} \right) \\ & - C_{q-2}^m \left[\frac{2}{3} x^2 f_{l'}(x) \frac{df_l(x)}{dx} - \frac{2(q-2)}{3} x f_{l'}(x) f_l(x) \right] \left(E_{[L(N+q-2)+l]} - E_{[L(q-2)+l]} \right) \Bigg\} dx \end{aligned} \tag{2.55}$$

Now, $\widehat{\mathbf{e}}_3 \cdot \mathbf{g}_0 = -g_0 \cos\theta$, therefore,

$$B\zeta = \sum_{n=|m|}^{N} \sum_{l=1}^{L} \left[\alpha^2 \sigma^2 (\sigma^2 - 1) + \beta g_0^2 (\sigma^2 - \cos^2\theta) \right] E_{[L(2N+q)+l]} f_l(x) Y_n^m. \tag{2.56}$$

We write EE3 as

$$\begin{aligned} EE3 = \sum_{l=1}^{L} \int \Big\{ & \frac{2}{3} \beta g_0^2 A_{q+2}^m x^2 f_{l'}(x) f_l(x) E_{[L(2N+q+2)+l]} \\ & + \frac{2}{3} \beta g_0^2 C_{q-2}^m x^2 f_{l'}(x) f_l(x) E_{[L(2N+q-2)+l]} \\ & + \left[\alpha^2 \sigma^2 (\sigma^2 - 1) + \beta g_0^2 (\sigma^2 - \frac{1}{3}) + \frac{2}{3} \beta g_0^2 B_q^m \right] x^2 f_{l'}(x) f_l(x) E_{[L(2N+q)+l]} \Big\} dx \end{aligned} \tag{2.57}$$

EE2 is written as

$$EE2 = 2\pi \sum_{l=1}^{L} \int x^2 f_{l'}(x) f_l(x) dx E_{[L(N+q)+l]} \tag{2.58}$$

Combining equations (2.55), (2.57), and (2.58), we finally write the Galerkin formulation of the entropy as

$$EE1 - \sigma^2(\sigma^2 - 1) EE2 - EE3 = 0 \tag{2.59}$$

2.6 The Boundary Conditions and the Inertial Modes

In this section, we will implement the boundary conditions involved in the Galerkin formulation of the 3PD. These conditions refer to the continuity of V_1, the normal component of the displacement, the normal component of the stress and the gravitational flux across the inner core boundary and core mantle boundary.

2.6.1 Inertial modes

Since the inner core and mantle are rigid, for the inertial modes of a rotating and neutrally stratified fluid core, the normal component of the displacement requires that

$$\widehat{\mathbf{n}} \cdot \mathbf{u} = \widehat{\mathbf{n}} \cdot \mathbf{u}_{IC} = 0 \tag{2.60}$$

The dimensionless gravitational potential is $V_1 = \sum \phi_n^m Y_n^m$. The continuity of V_1 is written as

$$V_1(b^-) = V_1(b^+) \tag{2.61}$$

where b^+ is the radius of the inner layer of the mantle, b^- the outer radius of the liquid core at the CMB. Using the spherical harmonics representation of the gravitational potential, the continuity in V_1 reduces to

$$\phi_n^m(b^-) = \phi_n^m(b^+) \tag{2.62}$$

Now, V_1 must be a solution of Laplace's equation in the mantle, so

$$\phi_n^m(r) = \frac{a_n^m}{r^{n+1}}, r > R_{mantle} \tag{2.63}$$

Since the mantle is rigid, then the continuity of $\widehat{\mathbf{n}}\cdot(\nabla V_1 - 4\pi G\rho\mathbf{u})$ accross the CMB becomes

$$\widehat{\mathbf{n}}\cdot\nabla V_1(b^-) = \widehat{\mathbf{n}}\cdot\nabla V_1(b^+) \tag{2.64}$$

Now

$$\widehat{\mathbf{n}}\cdot\nabla V_1(b^+) = -(n+1)\frac{a_n^m}{r^{n+2}} = -\frac{(n+1)}{r}\phi_n^m(b^+) \tag{2.65}$$

where $\widehat{\mathbf{n}} = \widehat{\mathbf{r}}$. Therefore using equation (2.63), we write

$$\widehat{\mathbf{n}}\cdot\nabla V_1(b^-) = -\frac{(n+1)}{r}\phi_n^m(b^-)Y_n^m \tag{2.66}$$

or

$$\frac{d\phi_n^m}{dr}(b^-) = -\frac{(n+1)}{r}\phi_n^m(b^-)Y_n^m \tag{2.67}$$

Therefore, with the omission of the Kronecker delta, the boundary condition involved in the Galerkin formulation of the Poisson equation is given as

$$\int f_{l'}(x)Y_q^m\widehat{\mathbf{n}}\cdot\nabla V_1 dS = -(q+1)xf_{l'}(x)f_l(b^+)E_{[}L(q)+l] \tag{2.68}$$

The term in equation (2.68) will be added to the elements $E[L(q)+l]$ of the matrix in the Poisson expansion. However, rigidity of the mantle requires that at the outer surface, the stress vanishes. Therefore, we write

$$\tilde{\tau} = -(p_1 + \mathbf{u}\cdot\nabla p_0)\tilde{\mathbf{1}} = 0 \tag{2.69}$$

or

$$p_1 + \mathbf{u}\cdot\nabla p_0 = p_1 + \mathbf{u}\cdot(\rho_0\mathbf{g}_0) = 0 \tag{2.70}$$

or

$$\frac{p_1}{\rho_0} + \mathbf{u} \cdot \mathbf{g}_0 = 0 \tag{2.71}$$

Therefore

$$\chi = -\mathbf{g}_0 \widehat{\mathbf{n}} \cdot \mathbf{u} = 0 \tag{2.72}$$

Since the mantle is rigid, this condition is automatically satisfied as the motion is parallel at the CMB. In the next section we present the boundary conditions implemented for the Galerkin formulation of the 3PD to solve for the Slichter frequencies.

2.6.2 Continuity of the normal component of the displacement

The continuity of the normal component of the displaced inner core at the ICB boundary requires that

$$\widehat{\mathbf{n}} \cdot \mathbf{u} = \widehat{\mathbf{n}} \cdot \mathbf{u}_{IC}. \tag{2.73}$$

Here $\mathbf{u}$ is the displacement of the fluid near the inner core boundary and $\mathbf{u}_{IC}$ the inner core displacement. We know that any point on a rigid solid body such as the inner core oscillates similar to a simple pendulum with a constant displacement amplitude in each direction. Assuming X_{max}, Y_{max}, Z_{max} are the maximun displacement amplitudes of any point of the inner core along the unit vectors $\widehat{\mathbf{e}}_1$, $\widehat{\mathbf{e}}_2$, $\widehat{\mathbf{e}}_3$ in a Cartesian coordinate system rotating with the Earth, with $\widehat{\mathbf{e}}_3$ along the rotation axis, we write

$$\mathbf{u}_{IC} = X_{max}\widehat{\mathbf{e}}_1 + Y_{max}\widehat{\mathbf{e}}_2 + Z_{max}\widehat{\mathbf{e}}_3 \tag{2.74}$$

We omit the time dependence $e^{\pm i\omega t}$ of the inner core displacement. It will be clear in chapter 3 why it is easier to defined $\mathbf{u}_{IC}$ in a Cartersian coordinate system. For a spherical Earth

$\widehat{\mathbf{n}} = -\widehat{\mathbf{r}}$. Therefore, for $l' = 1, .., L$ and $q = 1, ..., N$, we write the Galerkin formulation of the normal component of the inner core displacement in equation (2.31) as

$$ME1 = -\int_{ICB} f_{l'}(x)(X_{max}P_q^m \sin\theta\cos\phi + Y_{max}P_q^m \sin\theta\sin\phi + Z_{max}P_q^m \cos\theta)e^{-im\phi}dS \tag{2.75}$$

By using the fact that $\sin\theta = 2P_1^{-1}$, $\cos\theta = P_1^0$, $\sin\phi = -i\mathrm{Im}(e^{i\phi})$, and $\cos\phi = \mathrm{Re}(e^{-i\phi})$, where Re, and Im are the real and the imaginary parts of a complex number respectively, we rewrite equation (2.75) as

$$\begin{aligned} ME1 = -\int_{ICB} f_{l'}(x)(2X_{max}P_q^m p_1^{-1}e^{-i(m+1)\phi} - iY_{max}P_q^m P_1^1 e^{-i(m-1)\phi} \\ + Z_{max}P_q^m P_1^0 e^{-im\phi})dS \end{aligned} \tag{2.76}$$

Coupling the associated Legendre polynomial and integrating with respect to θ and ϕ, considering that only for $m = 1, 0, -1$, and $q = 1$ does the Kronecker symbol survive, we can rewrite equation (2.76) as

$$ME1 = \begin{cases} -\frac{4\pi}{3}x^2 f_{l'}(x)X_{max} & \text{if } m = -1, \text{and } q = 1, \\ \frac{8\pi i}{3}x^2 f_{l'}(x)Y_{max} & \text{if } m = 1, \text{and } q = 1, \\ -\frac{4\pi}{3}x^2 f_{l'}(x)Z_{max} & \text{if } m = 0, \text{and } q = 1. \end{cases} \tag{2.77}$$

By introducing new variables $X_0 = X_{max} + iY_{max}$ and $X_1 = X_{max} - iY_{max}$, we rewrite equation (2.77) as

$$ME1 = \begin{cases} -\frac{2\pi}{3}x^2 f_{l'}(x)(X_0 + X_1) & \text{if } m = -1, \text{and } q = 1, \\ \frac{4\pi}{3}x^2 f_{l'}(x)(X_0 - X_1) & \text{if } m = 1, \text{and } q = 1, \\ -\frac{2\pi}{3}x^2 f_{l'}(x)Z_{max} & \text{if } m = 0, \text{and } q = 1. \end{cases} \tag{2.78}$$

Considering the integration with respect to θ in the Galerkin formulation of the 3PD, we can therefore write the Galerkin formulation of the normal component of the displacement as

$$ME1 = \begin{cases} -x^2 f_{l'}(x)(X_0 + X_1) & \text{if } m = -1, \text{and } q = 1, \\ \frac{x^2}{2} f_{l'}(x)(X_0 - X_1) & \text{if } m = 1, \text{and } q = 1, \\ -x^2 f_{l'}(x) Z_{max} & \text{if } m = 0, \text{and } q = 1. \end{cases} \tag{2.79}$$

The above equations are then added to the Galerkin formulation of the momentum equation in section 2.4, which complete the system of $3LN$ unknowns, with 3 additional unknowns X_0, X_1, and Z_{max} to form a $(3NL + 3) \times (3NL + 3)$ matrix.

2.6.3 Continuity of the normal component of the gravitational flux

The continuity of the normal component of the gravitational flux at the inner core boundary requires that

$$\widehat{\mathbf{n}} \cdot (\nabla V_1 - 4\pi G \rho_0 \mathbf{u}) = \widehat{\mathbf{n}} \cdot (\nabla V_1^{'} - 4\pi G \rho_{IC} \mathbf{u}_{IC}), \tag{2.80}$$

Here $V_1^{'}$ is the inner core contribution for the perturbation in the gravitational potential. Rearranging the term involved in the continuity of the normal displacement, we write

$$PE3 = \int f_{l'}(x) Y_q^{m*} [4\pi G(\rho_0 - \rho_{IC}) \widehat{\mathbf{n}} \cdot \mathbf{u}_{IC} + \widehat{\mathbf{n}} \cdot \nabla V_1^{'}] dS \tag{2.81}$$

Since the continuity of $\widehat{\mathbf{n}} \cdot \mathbf{u}_{IC}$ is given in (2.79), we will follow Peng's work [64] to expand $\widehat{\mathbf{n}} \cdot \nabla V_1^{'}$. Therefore, we write

$$V_1^{'}(r) = G\rho_{IC} \int_{ICB} \mathbf{u}_{IC} \cdot \nabla(\frac{1}{R}) dV' \tag{2.82}$$

Using the divergence theorem, we then write

$$V_1^{'}(r) = G\rho_{IC}\int_{ICB}\frac{1}{R}\widehat{\mathbf{n}}\cdot\mathbf{u}_{IC}dS' \tag{2.83}$$

where R (see figure 3.3) is the distance from source point r' to field point r, which for $r' < r$ is expanded to two terms in Legendre polynomials as

$$\frac{1}{R} = \frac{1}{r} + \frac{r'}{r^2}\cos\theta$$

considering $\widehat{\mathbf{n}} = -\widehat{\mathbf{r}}$, at the ICB, where $\widehat{\mathbf{r}}$ is expanded in the Cartesian coordinate system. Substituting dS, and integrating with respect to ϕ, some of the component of the vector displacement $\mathbf{u}_{IC}$ vanishes, therefore, we write $V_1^{'}$ as

$$V_1^{'}(r) = -2\pi G\rho_{IC}Z_{max}\int\left(\frac{r'^2}{r}\sin\theta\cos\theta + \frac{r'^3}{r^2}\sin\theta\cos^2\theta\right)d\theta \tag{2.84}$$

Integrating with repect to θ, we rewrite equation (2.84) as

$$V_1^{'}(r) = -\frac{4\pi}{3}G\rho_{IC}\frac{a^3}{r^2}Z_{max}. \tag{2.85}$$

Here $G = \frac{G}{4\Omega^2}$, and using the dimensionless gradient $\nabla V_1^{'} = \frac{8\pi}{3}G\rho_{IC}\frac{a^3}{r^3}Z_{max}\widehat{\mathbf{r}}$, therefore, we write

$$\widehat{\mathbf{n}}\cdot\nabla V_1^{'} = -\widehat{\mathbf{r}}\cdot\nabla V_1^{'}(a) = -\frac{8\pi}{3}G\rho_{IC}Z_{max}. \tag{2.86}$$

By applying the Galerkin method in equation (2.81), where $l' = 1, .., L$ and $q = 1, .., N$, we write

$$\int_{ICB} f_{l'}(x)Y_q^{m*}\widehat{n}\cdot\nabla V_1^{'}dS = -\frac{8\pi}{3}G\rho_{IC}\int_{ICB}Z_{max}f_{l'}(x)Y_q^{m*}dS, \tag{2.87}$$

Following the same procedure as in section 2.6.2 and using the orthogonality relation associated to the integration with respect to θ, and ϕ, we can then write

$$\int_{ICB} f_{l'}(x) Y_q^{m*} \widehat{\mathbf{n}} \cdot \nabla V_1^{'} dS = \begin{cases} -\frac{8\pi}{3} G\rho_{IC} x^2 f_{l'}(x) Z_{max} & \text{if } m = 0, \text{and } q = 1; \\ 0 & \text{otherwise .} \end{cases} \tag{2.88}$$

Finally, the Galerkin formulation of the boundary condition involved in the Poisson equation is given by

$$PE3 = \begin{cases} -4\pi G(\rho_0 - \rho_{IC}) x^2 f_{l'}(x)(X_0 + X_1) & \text{if } m = -1, \text{and } q = 1, \\ 2\pi G(\rho_0 - \rho_{IC}) x^2 f_{l'}(x)(X_0 - X_1) & \text{if } m = 1, \text{and } q = 1, \\ -4\pi G(\rho_0 - \frac{1}{3}\rho_{IC}) x^2 f_{l'}(x) Z_{max} & \text{if } m = 0, \text{and } q = 1. \end{cases} \tag{2.89}$$

As for the normal component of the displacement, the condition in equation (2.89) will be added to the $3NL \times 3NL$ system from the Galerkin formulation of the 3PD. Finally, the boundary conditions developed add 3 additional rows with 3 unknowns to the 3PD, forming a $(3NL+3) \times (3NL+3)$ system. Therefore, we will solve a system of $(3NL+3) \times (3NL+3)$ elements to compute for the zeros of the determinant which correspond to the frequencies of the Slichter modes.

Chapter 3

DYNAMICS OF A RIGID INNER CORE

In this section, a simple Earth model will be adopted to solve for the frequencies of both the inertial and Slichter modes. To implement the IC equations of motion, we will use Newton's law to first show the contribution of all the forces involved in the dynamics of a prestress solid body such as the Earth. Thereafter, a vectorial inner core equations of motion derived from Newton's law will be projected along the unit vector of a Cartesian coordinate system.

3.1 Earth Model

The Earth model adopted in this study is a modified Preliminary Reference Earth Model (PREM) [16] with a rigid inner core and mantle, and an inviscid and neutrally stratified liquid core. The material properties such as density, compressional wave speed, mass

of the inner core (IC), and the mass of the Earth and so on, are from PREM (see Appendix A.3). We take the radius of the Earth to be $R = 6371$ km, the Earth rotation rate $\Omega = 7.292115 \times 10^{-5}$ s^{-1}, the gravitational constant $G = 6.6690941 \times 10^{-11}$ m^3 kg^{-1} s^{-2}. The density of the inner core ρ_{IC} and that of the fluid core ρ_0 near the inner core boundary will be directly calculated in the numerical computation using the data available from PREM. We will mainly study a modified PREM like Earth model where the density profile is a parabolic function of the radius of the inner core and a cubic function of radius in the outer core:

$$\rho_{IC} = a_1 + a_2 x^2$$

$$\rho_0 = b_1 + b_2 x + b_3 x^2 + b_4 x^3$$

where a_1, a_2, b_1, b_2, b_3, b_4 are PREM parameters (given in Appendix A.2) and x the radius normalized by the mean Earth's radius R = 6371 km. From the density profile of PREM in figure 3.1, it is easy to see the density jump across the ICB and the FC. We will first solve for the inertial modes of a rotating PREM with neutrally stratified fluid core, and thereafter compute numerically the frequencies of oscillation of the Slichter modes.

Figure 3.2 shows the inner core oscillating in a random direction from its initial position to the edge of a maximum shaded sphere. The shaded sphere is the maximum displacement of the inner core in any direction. In figure 3.2, the shaded area represents a small portion of the total fluid core interior of the Earth. Figure 3.3 shows the vector representation of the inner core in motion, including the vector relationships between the displaced inner core and the outer core system. In this diagram, a, $\mathbf{u}_{IC}$, ρ_0 and ρ_{IC} are

Figure 3.1: The density profile of PREM

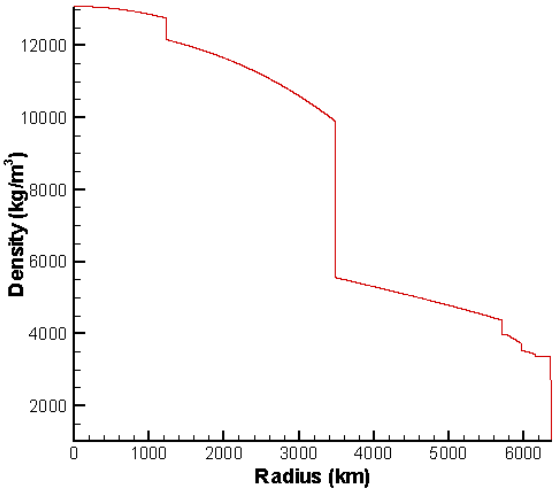

Figure 3.2: Inner core in random motion

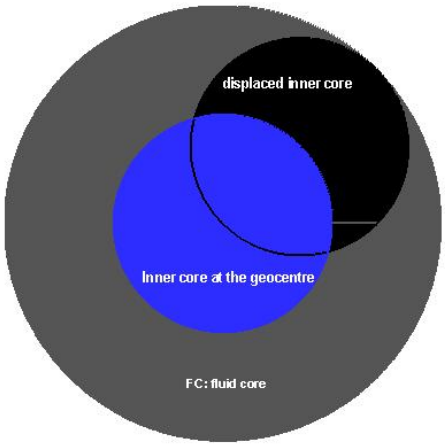

the radius of the inner core, the inner core displacement, the density of the shadded area or fluid core and the inner core density as discussed in Peng's thesis [25] .

Figure 3.3: Vectorial representation of the inner core in motion in the surrounding portion of the fluid core (shaded area). R, R', a, ρ_{IC}, ρ_0, u_{IC} and Ω are the field vector, the source vector, the radius of the inner core, the density of the inner core, the density of the fluid core, the inner core displacement and the Earth rotation rate respectively [25]

.

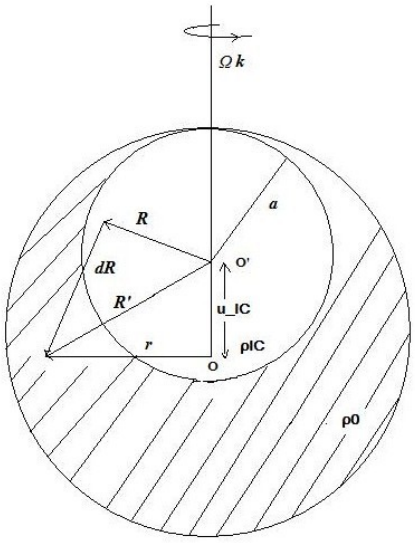

3.2 Gravitational and Pressure Contributions

In this section, we implement the effect of the gravitational force $\mathbf{F}_g$, and also the force due to the pressure contribution $\mathbf{F}_p$. The inner core experiences the gravitational force acting at any point interior to the inner core and the hydrodynamic pressure applied at the boundary. So as a starting model, we will use a non-rotating Earth, and recall the equation of motion of a deformable solid subject to hydrostatic prestress by Smylie and Mansinha (1971) [25, 52].

$$-\rho_{IC}\omega^2\mathbf{u}_{IC} = \nabla\cdot\tilde{\tau} + \rho_{IC}\nabla V_1 + \rho_{IC}\nabla(\mathbf{u}_{IC}\cdot\mathbf{g}_0) \tag{3.1}$$

Integrating over the inner core volume, we rewrite equation (3.1) as

$$-\omega^2 M_{IC}\mathbf{u}_{IC} = \int_{ICB} \nabla\cdot\tilde{\tau}dV + \rho_{IC}\int_{ICB}\nabla(V_1 + \mathbf{u}_{IC}\cdot\mathbf{g}_0)dV \tag{3.2}$$

where ω is the modal frequency and M_{IC} the mass of the inner core. By using the divergence theorem, we rewrite equation (3.2) as

$$-\omega^2 M_{IC}\mathbf{u}_{IC} = \int_{ICB}\tilde{\tau}\widehat{\mathbf{n}}_1 dS + \rho_{IC}\int_{ICB}(V_1 + \mathbf{u}_{IC}\cdot\mathbf{g}_0)\widehat{\mathbf{n}}_2 dS \tag{3.3}$$

where $\widehat{\mathbf{n}}_1$, and $\widehat{\mathbf{n}}_2$ are the outward pointing normal vector in the liquid core, and the inward pointing normal on the inner core. The stress in the liquid core is given as $\tilde{\tau} = -(p_1 + \rho_0\mathbf{u}\cdot g_0)\tilde{\mathbf{1}}$, By substituting the stress $\tilde{\tau}$, and after rearranging we rewrite equation (3.3) as

$$-\omega^2 M_{IC}\mathbf{u}_{IC} = -\int_{ICB}(P_1 + \rho_0\mathbf{u}\cdot g_0)\widehat{\mathbf{n}}_1 dS + \rho_{IC}\int_{ICB}(V_1 + \mathbf{u}_{IC}\cdot\mathbf{g}_0)\widehat{\mathbf{n}}_2 dS \tag{3.4}$$

Assuming that $\widehat{\mathbf{n}}_1 = \widehat{\mathbf{r}}$ at the FC, and $\widehat{\mathbf{n}}_2 = -\widehat{\mathbf{r}}$ at the inner core, and also $\mathbf{g}_0 = -g_0\widehat{\mathbf{r}}$ at the inner core, with the implementation of $\mathbf{u}\cdot\mathbf{g}_0 = \mathbf{u}_{IC}\cdot\mathbf{g}_0$ as in Peng's work [25], we then rewrite equation (3.4) as

$$-\omega^2 M_{IC}\mathbf{u}_{IC} = -\int_{ICB} P_1\widehat{\mathbf{r}}dS + g_0(a)(\rho_{IC} - \rho_0)\mathbf{u}_{IC}\cdot\int_{ICB}\widehat{\mathbf{r}}\widehat{\mathbf{r}}dS + \rho_{IC}\int_{ICB}V_1\widehat{\mathbf{r}}dS \tag{3.5}$$

substituting $P_1 = \rho_0\chi$ into equation (3.5), we finally can write both the contributions of gravitational force and pressure as

$$-\omega^2 M_{IC}\mathbf{u}_{IC} = -\rho_0\int_{ICB}\chi\widehat{\mathbf{r}}dS + \rho_{IC}\int_{ICB}V_1\widehat{\mathbf{r}}dS + (\rho_{IC} - \rho_0)\int_{ICB}\mathbf{u}_{IC}\cdot\mathbf{g}_0\widehat{\mathbf{r}}dS \tag{3.6}$$

where the force due to pressure is given by

$$\mathbf{F}_p = \rho_{IC}\int_{ICB}V_1\widehat{\mathbf{r}}dS - \rho_0\int_{ICB}\chi\widehat{\mathbf{r}}dS, \tag{3.7}$$

and the gravitational force as

$$\mathbf{F}_g = (\rho_{IC} - \rho_0) \int_{ICB} \mathbf{u}_{IC} \cdot \mathbf{g}_0 \widehat{\mathbf{r}} dS = -\omega_s^2 M_{IC} \mathbf{u}_{IC} \tag{3.8}$$

where $\omega_s^2 = \frac{4\pi}{3} G\rho_0(1-k)$, and $k = \frac{\rho_0}{\rho_{IC}}$.

3.3 Inner Core Equation of Motion

Newton's second law states that

$$\sum \mathbf{F} = M_{IC}\mathbf{a}, \tag{3.9}$$

where $\sum \mathbf{F}$ is the total force acting on the mass M_{IC} of the solid inner core, and $\mathbf{a}$ the total acceleration of the oscillating body. Now we use equations (3.7) and (3.8) for $\mathbf{F}_g$ and $\mathbf{F}_p$, from the above expansion, and with the addition of the action of the centrifugal force $\mathbf{F}_c = -(M_{IC} - M_0)\Omega^2 \widehat{\mathbf{e}}_3 \times (\widehat{\mathbf{e}}_3 \times \mathbf{u}'_{IC})$, and also the Coriolis force $\mathbf{F}_{Cor} = 2M_{IC}\Omega \widehat{\mathbf{e}}_3 \times \frac{d\mathbf{u}'_{IC}}{dt}$ where $\mathbf{u}'_{IC} = \frac{\mathbf{u}_{IC}}{R}$, $dS' = \frac{dS}{R^2}$ are the dimensionless inner core displacement and surface element, and χ', V_1' are the dimensionless trial functions defined in chapter 2. Here M_0 is the displaced fluid mass at the ICB. We next drop the prime sign for convenience and also the time dependence of the inner core displacement. then we rewrite equation (3.9) as

$$\begin{aligned}(-\omega^2 \mathbf{u}_{IC} + 2\Omega \widehat{\mathbf{e}}_3 \times \frac{d\mathbf{u}_{IC}}{dt}) M_{IC} = -\omega_s^2 M_{IC}\mathbf{u}_{IC} - (M_{IC} - M_0)\Omega^2 \widehat{\mathbf{e}}_3 \times (\widehat{\mathbf{e}}_3 \times \mathbf{u}_{IC}) \\ + \rho_{IC} \int_{ICB} V_1' \widehat{\mathbf{r}} dS - \rho_0 \int_{ICB} \chi \widehat{\mathbf{r}} dS \end{aligned} \tag{3.10}$$

However, dividing by $4\Omega^2 M_{IC}$, and choosing $\sigma = \frac{\omega}{2\Omega}$, $\eta = \frac{1-k}{4}$, $k = \frac{\rho_0}{\rho_{IC}}$, $\omega_s^2 = \frac{4\pi}{3}(1-k)$, $x_{IC} = \frac{r_{IC}}{R}$, $\gamma = \frac{\omega_s^2}{4\Omega^2}$ we rewrite equation (3.10) as

$$-\sigma^2 \mathbf{u}_{IC} + 2i\sigma \widehat{\mathbf{e}}_3 \times \mathbf{u}_{IC} = -\gamma \mathbf{u_{IC}} - \eta \widehat{\mathbf{e}}_{\mathbf{3}} \times (\widehat{\mathbf{e}}_{\mathbf{3}} \times \mathbf{u_{IC}}) + \frac{3}{4\pi x_{IC}^3} \int_{ICB} V_1 \widehat{\mathbf{r}} dS - \frac{3k}{4\pi x_{IC}^3} \int_{ICB} \chi \widehat{\mathbf{r}} dS, \tag{3.11}$$

We use the inner core displacement $\mathbf{u}_{IC} = X_{max}\widehat{\mathbf{e}}_1 + Y_{max}\widehat{\mathbf{e}}_2 + Z_{max}\widehat{\mathbf{e}}_3$. Thus, $\widehat{\mathbf{e}}_3 \times \mathbf{u}_{IC} = X_{max}\widehat{\mathbf{e}}_2 - Y_{max}\widehat{\mathbf{e}}_1$, and $\widehat{\mathbf{e}}_3 \times (\widehat{\mathbf{e}}_3 \times \mathbf{u}_{IC}) = -X_{max}\widehat{\mathbf{e}}_1 - Y_{max}\widehat{\mathbf{e}}_2$. We therefore expand the inner core equations of motion as

$$[(\gamma - \eta - \sigma^2)X_{max} - i\sigma Y_{max}]\widehat{\mathbf{e}}_1 + [(\gamma - \eta - \sigma^2)Y_{max} + i\sigma X_{max}]\widehat{\mathbf{e}}_2 + (\gamma - \sigma^2)Z_{max}\widehat{\mathbf{e}}_3 = \frac{3}{4\pi x_{IC}^3}\left[\int_{ICB} V_1 \widehat{\mathbf{r}} dS - k\int_{ICB} \chi \widehat{\mathbf{r}} dS\right], \tag{3.12}$$

From the earlier representation of the trial functions in equations (2.13)-(2.15) and with the substitution of $\widehat{\mathbf{r}} dS = x_{IC}^2(\sin\theta\cos\phi\widehat{\mathbf{e}}_1 + \sin\theta\sin\phi\widehat{\mathbf{e}}_2 + \cos\theta\widehat{\mathbf{e}}_3)\sin\theta d\theta d\phi$, we can write

$$[(\gamma - \eta - \sigma^2)X_{max} - i\sigma Y_{max}]\widehat{e}_1 + [(\gamma - \eta - \sigma^2)Y_{max} + i\sigma X_{max}]\widehat{e}_2 + (\gamma - \sigma^2)Z_{max} = \sum_{n=|m|}^{N}\sum_{l=0}^{L}(\frac{3}{4\pi x_{IC}}E_{[L(n)+l]} - \frac{3k}{4\pi x_{IC}}E_{[L(N+n)+l]})f_l(x)\int_{ICB}(\sin\theta\cos\phi\widehat{\mathbf{e}}_1 + \sin\theta\sin\phi\widehat{\mathbf{e}}_2 + \cos\theta\widehat{\mathbf{e}}_3)P_n^m e^{im\phi}\sin\theta d\theta d\phi, \tag{3.13}$$

We therefore rewrite the vector equation above as three scalar equations

$$\begin{cases} (\gamma-\eta-\sigma^2)X_{max} - i\sigma Y_{max} - \frac{3}{4\pi x_{IC}} \sum_{n=|m|}^{N} \sum_{l=0}^{L} (E_{[L(n)+l]} \\ -kE_{[L(N+n)+l]}) f_l(x) \int_{ICB} \sin^2\theta \cos\phi P_n^m e^{im\phi} d\theta d\phi = 0 \\ (\gamma-\eta-\sigma^2)Y_{max} + i\sigma X_{max} - \frac{3}{4\pi x_{IC}} \sum_{n=|m|}^{N} \sum_{l=0}^{L} (E_{[L(n)+l]} \\ -kE_{[L(N+n)+l]}) f_l(x) \int_{ICB} \sin^2\theta \sin\phi P_n^m e^{im\phi} d\theta d\phi = 0 \\ (\gamma-\sigma^2)Z_{max} - \frac{3}{4\pi x_{IC}} \sum_{n=|m|}^{N} \sum_{l=0}^{L} [E_{[L(n)+l]} \\ -kE_{[L(N+n)+l]}] f_l(x) \int_{ICB} \cos\theta \sin\theta P_n^m e^{im\phi} d\theta d\phi = 0. \end{cases} \tag{3.14}$$

Using the orthogonality relation of the Legendre polynomials in equation (2.26), we write equation (3.14) as follows:

For $m = -1$ and $q = 1$

$$\begin{cases} (\gamma-\eta-\sigma^2)X_{max} - i\sigma Y_{max} - \frac{1}{x_{IC}} \sum_{l=0}^{L} (E_{[L(q)+l]} - kE_{[L(N+q)+l]}) f_l(x) = 0 \\ (\gamma-\eta-\sigma^2)Y_{max} + i\sigma X_{max} = 0 \\ (\gamma-\sigma^2)Z_{max} = 0 \end{cases} \tag{3.15}$$

For $m = 1$ and $q = 1$

$$\begin{cases} (\gamma-\eta-\sigma^2)X_{max} - i\sigma Y_{max} = 0 \\ (\gamma-\eta-\sigma^2)Y_{max} + i\sigma X_{max} + \frac{2i}{x_{IC}} \sum_{l=0}^{L} (E_{[L(q)+l]} - kE_{[L(N+q)+l]}) f_l(x) = 0 \\ (\gamma-\sigma^2)Z_{max} = 0 \end{cases} \tag{3.16}$$

For $m = 0$ and $q = 1$,

$$\begin{cases} (\gamma - \eta - \sigma^2)X_{max} - i\sigma Y_{max} = 0 \\ (\gamma - \eta - \sigma^2)Y_{max} + i\sigma X_{max} = 0 \\ (\gamma - \sigma^2)Z_{max} - \frac{1}{x_{IC}} \sum_{l=0}^{L} (E_{[L(q)+l]} - kE_{[L(N+q)+l]}) f_l(x) = 0 \end{cases} \tag{3.17}$$

Considering the variables X_0 and X_1 adopted in the boundary conditions in sections 2.6.2 and 2.6.3, we rewrite the inner core equation of motion as follow:

For $m = -1$ and $q = 1$,

$$\begin{cases} (\gamma - \eta - \sigma - \sigma^2)X_0 + (\gamma - \eta + \sigma - \sigma^2)X_1 - \frac{2}{x_{IC}} \sum_{l=0}^{L} (E_{[L(q)+l]} - kE_{[L(N+q)+l]}) f_l(x) = 0 \\ (\sigma - \gamma + \eta + \sigma^2)X_0 + (\sigma + \gamma - \eta - \sigma^2)X_1 = 0 \\ (\gamma - \sigma^2)Z_{max} = 0 \end{cases} \tag{3.18}$$

For $m = 1$ and $q = 1$,

$$\begin{cases} (\gamma - \eta - \sigma - \sigma^2)X_0 + (\gamma - \eta + \sigma - \sigma^2)X_1 = 0 \\ (\sigma - \gamma + \eta + \sigma^2)X_0 + (\sigma + \gamma - \eta - \sigma^2)X_1 + \frac{4}{x_{IC}} \sum_{l=0}^{L} (E_{[L(q)+l]} - kE_{[L(N+q)+l]}) f_l(x) = 0 \\ (\gamma - \sigma^2)Z_{max} = 0 \end{cases} \tag{3.19}$$

For $m = 0$ and $q = 1$,

$$\begin{cases} (\gamma - \eta - \sigma - \sigma^2)X_0 + (\gamma - \eta + \sigma - \sigma^2)X_1 = 0 \\ (\sigma - \gamma + \eta + \sigma^2)X_0 + (\sigma + \gamma - \eta - \sigma^2)X_1 = 0 \\ (\gamma - \sigma^2)Z_{max} - \frac{1}{x_{IC}} \sum_{l=0}^{L} (E_{[L(q)+l]} - kE_{[L(N+q)+l]}) f_l(x) = 0 \end{cases} \tag{3.20}$$

For the computations of the Slichter frequencies, these equations will be added to the expanded radial component of the 3PD discussed earlier in chapter 2 to form a square matrix, for which any numerical method can be used to solve for the zeros of the determinant, which correspond to the frequencies of the Earth's normal modes.

Chapter 4

RESULTS AND DISCUSSIONS FOR A SPHERICAL EARTH

In this section, we first compute the frequencies and displacement eigenfunctions for some of the inertial modes of a neutrally stratified core for which the results are known in order to check the validity our results. We will then present and discuss the results for the frequencies and eigenfunctions of the Slichter modes for the same model .

4.1 Matrix Implementation and Eigenvalues

The matrix to be solved for the eigenvalues of a rotating, compressible and stratified fluid core is obtained by the implementation of the Galerkin formulation for the numerical solution of the 3PD. There are 3 equations and 3 unknowns. We have shown that the use of the orthogonality relation among spherical harmonics leads to the removal of the θ and ϕ dependence of field variables. The r dependence of one of the terms in the series expansion

is linked to every other components in the same series via the chain relations in equations (2.44)-(2.45).

For each q there corresponds N_{max} terms from expanding the r components. Each equation involves $3 \times N \times L$ unknowns and the application of a Galerkin method ensures that there are $3 \times N \times L$ equations. The expansion of the 3PD shows that there are 2 independent chains representing the dynamics of the core, one links the odd degree spherical harmonics, the other, the even. For the non-trivial solution of the set of Galerkin equations, then the determinant of the coefficient matrix must vanish. An example of the shape of the matrix involved in this study is given by assuming $L_{max} = 3$, $N_{max} = 1$ where L_{max} and N_{max} represent the truncation level of the Legendre polynomials and the highest degree of the spherical harmonics. Then, for the above choice, a 9×9 matrix is shown below for even values of q.

$$\begin{bmatrix} u_{11} & u_{12} & u_{13} & v_{11} & v_{12} & v_{13} & 0 & 0 & 0 \\ u_{21} & u_{22} & u_{23} & v_{21} & v_{22} & v_{23} & 0 & 0 & 0 \\ u_{31} & u_{32} & u_{33} & v_{31} & v_{32} & v_{33} & 0 & 0 & 0 \\ w_{11} & w_{12} & w_{13} & u_{11} & u_{12} & u_{13} & v_{11} & v_{12} & v_{13} \\ w_{21} & w_{22} & w_{23} & u_{21} & u_{22} & u_{23} & v_{21} & v_{22} & v_{23} \\ w_{31} & w_{32} & w_{33} & u_{31} & u_{32} & u_{33} & v_{31} & v_{32} & v_{33} \\ 0 & 0 & 0 & w_{11} & w_{12} & w_{13} & u_{11} & u_{12} & u_{13} \\ 0 & 0 & 0 & w_{21} & w_{22} & w_{23} & u_{21} & u_{22} & u_{23} \\ 0 & 0 & 0 & w_{31} & w_{32} & w_{33} & u_{31} & u_{32} & u_{33} \end{bmatrix} \times \begin{bmatrix} E_1 \\ E_2 \\ E_3 \\ E_4 \\ E_5 \\ E_6 \\ E_7 \\ E_8 \\ E_9 \end{bmatrix} = 0$$

Here w_{ij}, u_{ij}, v_{ij} are the coefficients attached to the unknowns $E[L(q-2)+l]$, $E[L(q)+l]$ and $E[L(q+2)+l]$ in the Galerkin formulation of the 3PD respectively. The inner product of trial functions and the terms in the Galerkin formulation of the 3PD gives these coefficients for different values of $l = 1...L$, and $l' = 1...L$ and different values of $q = 1...N$. The matrix above is given by first choosing $L_{max} = 3$. Since we are dealing with 3 equations, then for each incrementation of l', 3 rows are formed. The incremenation of l contributes in forming the columns of the matrix, after full incrementation a 9×9 matrix is finally obtained.

4.2 Inertial Modes of a Rotating Fluid Core

To compute the desired frequencies, we first fixed the value of N_{max} and then increase L_{max} until the computed frequency shows convergence, then we will increase N_{max} and repeat the process until the computed frequency converges for any N_{max} or L_{max}. Here we compute some of the low order modes for $m = 0$, and $m = 1$ for the inertials modes of a spherical, and neutrally stratified and compressible PREM model. Then later the same techniques are applied for the computation of the Slichter modes for $m = 0, 1, -1$.

We search for the zeros of the determinant of the coefficient matrix in the frequency range $|\sigma| \leq 1$ for $m = 1$, and $0 \leq \sigma \leq 1$ for $m = 0$. This is because the modes are symmetric for $m = 0$, and the dimensionless frequencies of the inertial modes satisfy $|\sigma| \leq 1$. We adopt Greenspan's (1968) notation $(n, k, m\ )$ for mode labelling [65], where for each n and m, there corresponds k modes, (n, k, m) refers to the degree of the spherical harmonics, the order of the mode and the azimuthal wavenumber, respectively. The orders of the modes are according to the size of their frequencies. For the same azimuthal number m, and n

the smallest modal frequency is labelled $(n, 1, m)$. To avoid repetition, we will only select positive modes for $m = 0$. This is because the only difference is that one is prograde and the other retrograde but the frequencies are the same. However, for $m = 1$ there is no symmetry, therefore, every possible frequency will be reported.

Table 4.1: Test of convergence of some of the low order modes for a neutrally stratified PREM Earth model

Mode	N=6, L=12	N=8, L=16	N=10, L=16	N=12, L=18	N=12, L=20
(4, 1, 0)	0.6648	0.6639	0.6643	0.6644	0.6644
(2, 1, 1)	0.5000	0.5000	0.5000	0.5000	0.5000
(4, 3, 1)	0.8527	None	0.8537	0.8530	0.8530
(6, 4, 1)	0.6576	0.6572	0.6573	0.6574	0.6574

In table 4.1, we show the trend of convergence for some low order modes for different truncations levels. It is shown that for a higher level of truncation $L = 16$ of the Legendre polynomial, the modes converge and are stable without fluctuating for the mode (4, 1, 0). However, the mode (2, 1, 1) converges so fast and shows no fluctuation starting for low level of truncation $L = 3$, $N = 1$. Furthermore, for the modes (4, 3, 1) and (6, 4, 1) the trend of convergence is up to 3 decimal points from the level of truncation $(16, 10)$, $(18, 12)$, and $(20, 12)$ respectively. The results shown in table 4.2 represent the frequencies of more modes of a shell. Columns 2, and 3 represent both the dimensionless frequencies $\sigma = \frac{\omega}{2\Omega}$ for a compressible shell studied for a neutrally stratified fluid core by Seyed-Mahmoud et al., 2007 [35], and studied in this thesis respectively. We should note that the values in column

Table 4.2: Frequencies of some of the low order modes of a rotating, compressible and neutrally stratified fluid core (column 1), σ_{BSM} (Seyed-Mahmoud et. al., 2007) in column 2, in column 3 those computed in this work, and the truncation level in column 4.

Mode	σ_{BSM}	σ	N_{max}, L_{max}
(4, 1, 0)	0.664	0.664	12, 18
(6, 1, 0)	0.473	0.472	14, 23
(6, 2, 0)	0.833	0.834	12, 25
(2, 1, 1)	0.500	0.500	3, 5
(4, 2, 1)	0.304	0.304	10, 16
(4, 3, 1)	0.852	0.853	12,18
(5, 4, 1)	0.932	0.933	12, 25
(6, 1, 1)	-0.703	-0.702	12, 18
(6, 4, 1)	0.657	0.657	12, 18
(7, 2, 1)	-0.434	-0.434	10, 23
(7, 5, 1)	0.740	0.740	8, 16

3 were recorded and rounded off to 3 significant figures. The level of truncation is shown in column 4 for the modes studied in this thesis. It is shown a high agreement between our results in column 3 and column 4 are taken from Seyed-Mahmoud et al. (2007) [35].

4.3 Eigenfunctions of Some of the Inertial Modes of the Fluid Core

Here we present some of the eigenfunctions corresponding to the frequencies shown in table 4.2. The eigenfunctions were plotted, as previously mentioned, by the help of the engineering software package TecPlot 10 (re: software company AMTEC ENGINEERING, INC.). In figure 4.1 (a-g), we show the displacement eigenfunctions for the (2, 1, 1),

Figure 4.1: Displacement patterns for (a): the (2, 1, 1), (b): (4, 1, 0), (c): (4, 2, 1), (d): (4, 3, 1), (e): (6, 1, 1), (f): (6, 4, 1) and (g): (7, 5, 1) modes of PREM in a meridional plane, $\phi = 0$, for a compressible shell.

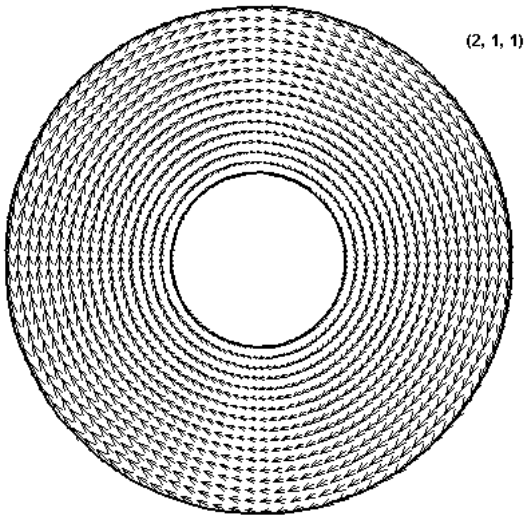

(a)

(4, 1, 0), (4, 2, 1), (4, 3, 1), (6, 1, 1), (6, 4, 1) and (7, 5, 1) inertial modes of a modified PREM. In most figures the displacement is parallel to the boundaries. It is clear that the overall displacement patterns are regular, but there are some discrepancies in a few spots on some plots mostly originating from truncation. For some of the modes, the displacement

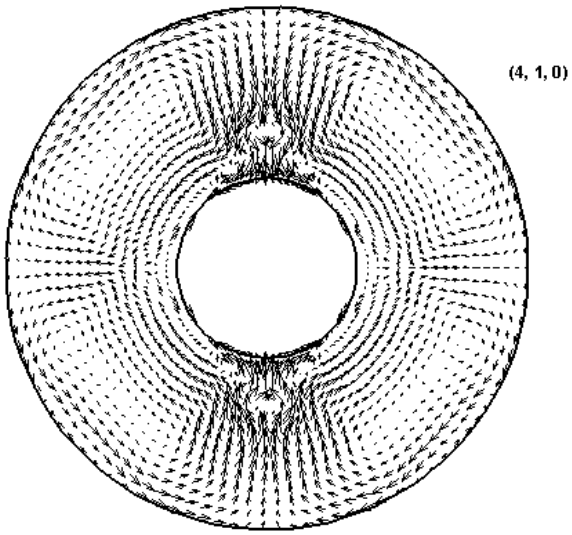

(b)

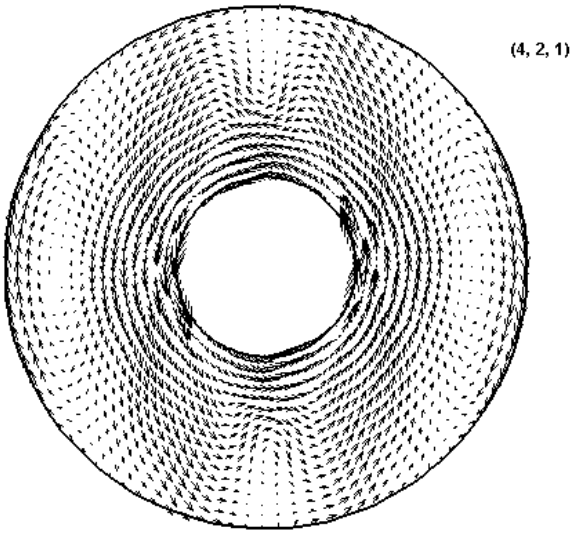

(c)

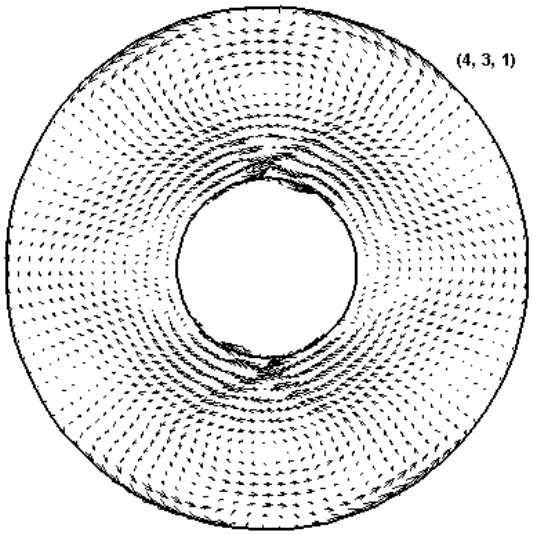

(d)

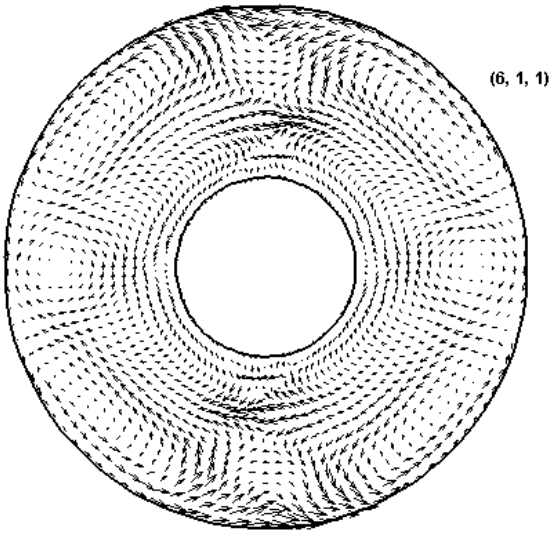

(e)

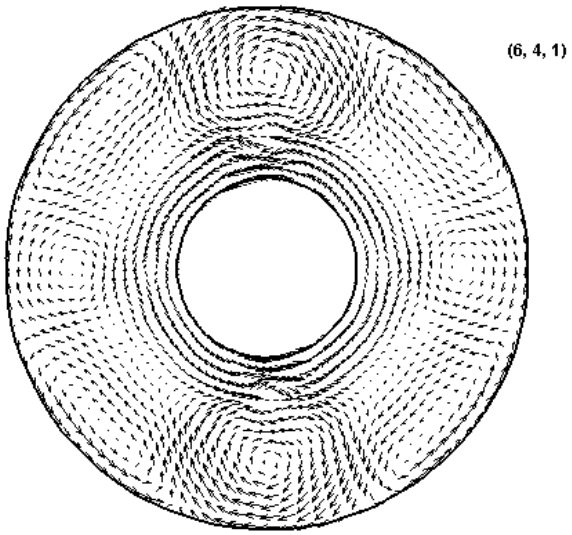

(f)

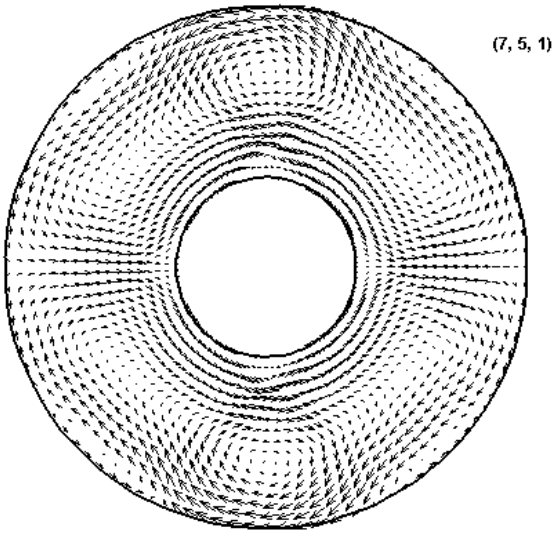

(g)

patterns are forced to be parallel to the boundaries, especially at the ICB. Therefore, the mathematical treatment may not be adequate for these modes. Most of the patterns shown in these figures are very similar to those studied by Poincaré [65]. For the (2, 1, 1) mode, the displacement patterns are parallel to the boundary. This may be the reason why the convergence is so fast.

4.4 The Slichter Modes

To solve for the frequencies of the Slichter triplets, we will first highlight how to implement the matrix generated from the expansion of the 3PD and the inner core equations of motion previously discussed. Next we will present and discuss the results of the Earth's Slichter frequencies for a spherically and neutrally stratified fluid core, with a rigid inner core, for both non-rotating and rotating cases.

In this section we are dealing with a $(3NL + 3) \times (3NL + 3)$ square matrix, in which $3NL \times 3NL$ coefficients arise from the implementation of the 3PD as previously shown during the study of the inertial modes. However, for a complete set, the inner core equations of motion must also be added. The boundary conditions provide three extra unknowns X_0, X_1, and Z_{max} from the momentum and Poisson equations, via the implementation of the surface integral in the Galerkin formulation of the 3PD.

On the search of the Slichter triplets, we show in chapters 2 and 3 that the Slichter frequencies and displacements correspond to the azimuthal wavenumbers 1, -1, and 0. In chapters 2 and 3 we also showed that the spherical harmonics of degree 1 ($q = 1$ in chapter 2 in equations (2.79) and (2.89), also in chapter 3 in equations (3.18)-(3.20)) correspond

to the Slichter triplets. Therefore, the chain in equations (2.44)-(2.45) which corresponds to the odd values for the degree of the spherical harmonics describes the Slichter triplet. However, we change the range of the dimensionless modal frequency σ to $1.5 \leq \sigma \leq 6$ for a search of periods between 2 and 8 hours.

We use the computer language FORTRAN 95 and the IMSL library. There were different internal routines from International Mathematics and Statistics Library (IMSL) [66] used for the numerical computation of the frequencies and displacements involved for this study. In this study, the desired absolute error in the numerical integration of radial functions is ERRABS= 10^{-8}. However, the chosen tolerance is Tol=10^{-7}. This means that the non-trivial roots of the determinant of $(3 \times N \times L + 3)$ system are found accurate to 10^{-7}. The integrations with respect to r are evaluated using the IMSL internal double precision routine DQ2AG [66] for the computation of all the integral terms in the mathematical equations of this work. The routine DQ2AG integrates by subdividing the interval $[a, b]$ using a globally adaptive scheme to reduce the absolute error based on the Kronrod rule to estimate the integral error over each subinterval [66].

We basically use a technique similar to the bisection method. Once the value of the determinant changes sign for two consecutive values of σ, there exists a root of the determinant. Assuming that $[a, b]$ is the interval in which the determinant changes sign, the search of modal frequencies is conducted from b to a searching back and forth with a specific value of step size which gets smaller in each iteration until the tolerance is satisfied.

We first present the convergence scheme of possible modes as discussed earlier, for both a non-rotating and rotating case for a neutrally stratified and compressible PREM

model, and discuss the procedure of mode selection. Once a frequency is converged, the frequency and the associated degrees of convergence, L and N are reported. The same procedure is used as in the study of the inertial modes. In tables 4.4, 4.5 and 4.6, we show the convergence for the azimuthal number $m = 0$, $m = 1$, and $m = -1$ respectively. For consistency with the literature, we report the period of the mode, rather than the frequency, $T = \frac{2\pi}{f}$.

Table 4.3: Convergence of the periods of the Slichter central mode (m=0)(hr) for a neutrally stratified PREM: non-rotating case.

N, L	N=3, L=5	N=3, L=7	N=3, L=10	N=3, L=15
m=0	NA	5.254	NA	5.254
N, L	N=4, L=7	N=4, L=9	N=4, L=11	N=4, L=15
m=0	5.254	5.254	5.254	5.254
N, L	N=7, L=9	N=7, L=10	N=7, L=12	N=7, L=15
m=0	5.254	5.254	5.254	5.254
N, L	N=8, L=14	N=8, L=16	N=8, L=18	N=8, L=20
m=0	5.254	5.254	5.254	5.254
N, L	N=10, L=14	N=10, L=16	N=10, L=18	N=10, L=20
m=0	5.254	5.254	5.254	5.254
N, L	N=12, L=14	N=12, L=16	N=12, L=18	N=12, L=20
m=0	5.254	5.254	5.254	5.254

In table 4.3 we show the convergence of the central mode (m=0) for a neutrally

stratified PREM for a non-rotating Earth. The highest level of truncation chosen $N = 3$ and $L = 5$. By increasing the complexity of the Legendre functions from $L = 5...15$, and for a fixed value of N, the value 5.254 h shows the trend of a potential mode. Moreover, by increasing from $N = 4$ to $N = 12$, and keeping in mind that L is increased for any fixed N in the above range, the mode listed above does not show fluctuation computed up to 3 decimal points in the table of convergence, for the central mode of a non-rotating, and spherically stratified PREM model. However a close analysis of table 4.3, and looking at the highest level truncations corresponding to $N = 10$ and $N = 12$, we can conclude that the period of the central mode has converged up to 3 decimal places and will be reported as 5.254 h.

Table 4.4: Convergence of the periods of the Slichter modes (hr) for a neutrally stratified PREM: rotating case.

N, L	N=3, L=5	N=3, L=8	N=3, L=10	N=3, L=12
m=0	5.254	5.254	5.254	5.254
	3.651	3.651	3.651	3.651
	3.455	3.455	NA	3.455
m=1	4.976	4.976	4.976	4.976
	4.376	4.376	4.376	4.376
	3.426	3.426	3.426	3.426
m=-1	5.874	5.875	5.875	5.875
	4.376	4.376	4.376	4.376
	3.870	3.870	3.870	3.870

Table 4.5: Convergence of the periods of the Slichter modes (hr) for a neutrally stratified PREM: rotating case (continued).

N, L	N=4, L=7	N=4, L=9	N=4, L=12	N=4, L=14
m=0	5.254 3.651 3.455	5.254 3.651 NA	5.254 3.651 3.455	5.254 3.651 3.457
m=1	4.976 4.376 3.426	4.976 4.376 3.426	4.976 4.376 3.426	4.976 4.376 3.426
m=-1	5.875 4.376 3.870	5.875 4.376 3.870	5.875 4.376 3.870	5.875 4.376 3.870
N, L	N=7, L=10	N=7, L=12	N=7, L=14	N=7, L=16
m=0	5.254 3.651 3.455	5.254 3.651 3.455	5.254 3.651 3.457	5.254 3.651 NA
m=1	4.976 4.376 3.426	4.976 4.376 3.426	4.976 4.376 3.426	4.976 4.376 3.426
m=-1	5.875 4.376 3.870	5.875 4.376 3.870	5.875 4.376 3.870	5.875 4.376 3.870

Table 4.6: Convergence of the periods of the Slichter modes (hr) for a neutrally stratified PREM: rotating case (continued).

N, L	N=8, L=14	N=8, L=16	N=8, L=18	N=8, L=20
m=0	5.254	5.254	5.254	5.254
	3.651	3.651	3.651	3.651
	3.455	3.455	3.455	3.455
m=1	4.976	4.976	4.976	4.976
	4.376	4.376	4.376	4.376
	3.426	3.426	3.426	3.426
m=-1	5.875	5.875	5.875	5.875
	4.376	4.376	4.376	4.376
	3.870	3.870	3.870	3.870

Following the procedure described above for the central mode, we show in tables 4.4, 4.5, 4.6 and 4.7, the convergence of the periods of the Slichter modes of a rotating spherical Earth for a neutrally stratified PREM. In column 1 are presented the azimuthal number $m = 0, 1, -1$ which are associated with the central, retrograde, and prograde modes respectively. In column 2, the roots of the displayed level of truncation are given. We can see three possible modes listed for each truncations, starting from $N = 3, L = 5$ until $N = 7$, and $L = 10$, for the mode with period 5.254 h. However, increasing $N = 8$, and choosing $L = 14, 16, 18, 20$, the suspected eigenvalue 5.254 h shows stability. To ensure for the convergence of this mode, we increase $N = 10$ and also increment $L = 16, 18, 20$. As shown in table 4.6, the same mode does not fluctuate, therefore we consider that it is

Table 4.7: Convergence of the periods of the Slichter modes (hr) for a neutrally stratified PREM: rotating case (continued).

N, L	N=10, L=16	N=10, L=18	N=10, L=20
m=0	5.254	5.254	5.254
	3.651	None	None
	3.455	None	None
m=1	4.976	4.976	4.976
	4.376	4.376	4.376
	3.426	3.426	3.426
m=-1	5.875	5.875	5.875
	4.376	4.376	4.376
	3.870	3.870	3.870

converged. We then assigned it as the mode representing the central mode ($m = 0$).

From both the convergence for the central mode of a non-rotating case and those for a rotating and neutrally stratified PREM model presented above, we recover all the three modes corresponding to the Slichter triplets, for a rotating Earth model. We are also presented with some false roots in the table of convergence. However, the false roots either disappear or change considerably when N_{max} or L_{max} are increased, i.e. there is no convergence. In table 4.7 we present the departure from the axial mode ($m = 0$) to the prograde ($m = -1$) and the retrograde ($m = 1$) modes.

Table 4.8: Possible Slichter eigenperiods corresponding to the prograde ($m = -1$) and retrograde ($m = 1$) modes (column 2) and their departure from the central mode (column 3) for a rotating and neutrally stratified PREM model.

m	Slichter eigenvalues (hr)	% difference
1	4.976	0.28
1	4.376	0.88
1	3.426	1.83
-1	5.875	0.62
-1	4.376	0.88
-1	3.870	1.38

Table 4.9: Schliter's eigenperiods (hr) for spherical and neutrally stratified PREM, for both a non-rotating and rotating modes.

m	Slichter eigenvalues (hr)
0	5.254
1	4.976
-1	5.875
Non rotating	5.254

Following the convergence scheme shown in tables 4.4, 4.5, and 4.6, based on the restriction that the departure of the central mode is the smallest from possible modes shown in table 4.7, we therefore present in table 4.8, a final selection of the Slichter triplet corresponding to the central (m=0), prograde (m=-1), and retrograde (m=1) for a spherical and neutrally stratified rotating (rows 2, 3, and 4), and for the non-rotating (in 5 row) PREM. As a further check of the validity of our results, we compare them with those studied

for a stratified fluid core of the PREM by Peng [25] using the two potential description (TPD), and the subseismic approximation. They are presented in table 4.9. In column 1 the method used, from the second to fourth column, the value of m for a rotating and spherical Earth model, and finally the fifth column, the mode of a non-rotating case is presented.

Table 4.10: Slichter eigenperiods (hr) comparison for a spherically and neutrally stratified liquid core, for a rotating and non-rotating Earth, using differents methods.
3PD: results of this thesis.
TPD: Two Potential Description by Peng (1995).
SSA: Subseismic approximation by Peng (1995).

Method	m=0	m=1	m=-1	non-rotating
3PD	5.254	4.976	5.875	5.254
TPD	5.303	4.759	5.972	5.413
SSA	5.301	4.759	5.969	5.411
% diff 3PD-TPD	0.92	4.45	1.63	2.98
% diff 3PD-SSA	0.89	4.45	1.58	2.94

Note that the percentage difference in rows 5 and 6 are evaluated using the formula %diff=|3PD-TPD|/average (3PD, TPD), and in the second case TPD is replaced by SSA. Generally speaking, the error between the computed modes for the 3PD and TPD for the rotating PREM is about 5%, and the maximum difference appears in retrograde mode (m=+1) and the minimun difference in the central mode (m=0), with respective values of about 4.45% and 0.92%. The difference for the prograde mode is about 1.63%. Note that the percentage difference between the 3PD and SSA is still less than 5% following the same

trend for the prograde and retrograde mode with the discrepancy of about 4.45% and 0.89% respectively. The difference in retrograde is about 1.58%. However, the percentage difference between the SSA and TPD against our results for the central mode for a non-rotating PREM is about 3%. The difference between the results from this work and those from Peng arises from Peng's use of an elastic inner core and mantle while we consider them to be rigid, and also some of the differences may be from the use of the TPD rather than the 3PD.

We next compared the results of this study with the computed frequency in Wu and Rochester [67]. They used PREM, as in this thesis, and solved the TPD using a Galerkin formulation, but in their study the trial functions satisfy a priory the boundary conditions. Note that the percentage differences were calculated as above. In table 4.11 we show our results along with those of Wu and Rochester [67].

Table 4.11: Slichter eigenperiods (hr) comparison of different authors.
3PD: results of this thesis using the 3PD.
W-TPD: Wu and Rochester (1994) results, using TPD and Galerkin method with boundary conditions satisfied a priori.

Authors and methods	m=0	m=1	m=-1	non-rotating
3PD	5.254	4.976	5.875	5.254
W-TPD	5.310	4.766	5.979	5.420
% W-3PD	1.0	4.3	1.7	3.1

Table 4.11 shows a good agreement of about 1% between the eigenperiods calculated in this thesis and those studied by Wu and Rochester [67] for the central or polar mode (m=0). However, the eigenperiods associated to the retrograde (m=+1), and prograde (m=-

1) are 1.7%, and 4.3% shorter than those of Wu and Rochester [67]. For the non-rotating case a fair agreement of about 3% between the two methods. This small discrepancy may be due to the way we handle the boundary conditions. We use the natural character of the boundary conditions while in Wu and Rochester [67], the continuity of the scalar field was set in a way that the trial functions satify a priori the boundary conditions exactly.

We next compared the results of this thesis with the results of Rieutord [57]. We both use the same inner core equations of motion deduced using Newton's Law. Moreover, the Earth model adopted in his work is PREM with neutrally stratified and inviscid liquid core. The difference in Rieutord's model is that he used a viscous fluid core of PREM, and also in his study the dynamics of the fluid core was treated using the SSA as compared to the 3PD in this work. We show in table 4.12, the comparison of the results of this study and those of Rieutord [57]. In column 1, the method used, and from columns 2-4, the frequencies for different azimuthal numbers for both methods for a rotating case are given. However, in column 5 is presented the mode for a non-rotating case.

Table 4.12: Slichter eigenperiods (hr) compared for different representation of the motion of the fluid
3PD: results of this thesis using the 3PD.
MR-SSA: Michel Rieutord (2002) results, using SSA in the fluid side and IC equation of motion.

Authors and methods	m=0	m=1	m=-1	non-rotating
3PD	5.254	4.976	5.875	5.254
MR-SSA	4.240	3.833	4.614	4.240
% 3PD-MR	23.8	25.9	24.0	23.8

From table 4.12, the axial, prograde and retrograde modes in this work are 23.8%, 25.9% and 24% respectively larger than those studied by Rieutord [57]. However, the results for a non-rotating case is 23.8% larger (which is the same as for the central mode). The lowest discrepancy is shown in the non rotating case, and the largest in the rotating case for the retrograde mode. The larger discrepancy between the result of this work and those of Rieutord maybe due to the consideration of the SSA at the fluid side, and also by the treatment of the fluid as viscous. Moreover, the disagreement between Rieutord and our work may arise by the choice of constant density of 12 g/cm^3 instead of 12.166 g/cm^3 for the fluid core and 13 g/cm^3 instead of 12.763g/cm^3 for the inner core near the ICB. In addition, this disagreement maybe partially due to the use of toroidal and spheroidal representations of the displacement field.

4.5 Slichter's Eigenfunctions

In this section we will present the displacement patterns of the Slichter modes for a rotating and non-rotating spherical and neutrally stratified fluid core of PREM. The procedure to compute the eigenfunctions is as follows. After the eigenperiods have been obtained, we solve for the coefficients of the trial functions using the IMSL internal subroutine DLSARG. Note that DLSARG is a double precision IMSL version of LSARG, which solves a system of linear algebraic equations with real coefficients using iterative refinement via LU factorization [66]. They are used to compute the displacement patterns, and by the help of the engineering software package TecPlot 10 the modes associated to the Slichter triplets are plotted.

The linear and algebraic equation used to develop the algorithm of the displacement vector is based on the formula for a neutrally stratified fluid core of the PREM as in Seyed-Mahmoud et al. [35], namely

$$\sigma^2(\sigma^2 - 1)\mathbf{u} = \tilde{\mathbf{\Gamma}}_{\mathbf{P}} \cdot \nabla(\chi - V_1), \tag{4.1}$$

where $\mathbf{u}$, σ, χ and V_1 are the fluid motion during Slichter oscillations, the Slichter frequency associated to the displacement $\mathbf{u}$, the trial functions associated to pressure, and the gravitational potential.

Figure 4.2: Displacement patterns of the the fluid motion during the Slichter oscillation associated to (a): the central ($\sigma = 5.254028$ h), (b): prograde ($\sigma = 5.875292$ h) , and (c): retrograde ($\sigma = 4.976512$ h) modes for a neutrally stratified core, in a meridional plane, $\phi = 0$, for a compressible shell. The axis of rotation is perpendicular to the horizontal plane

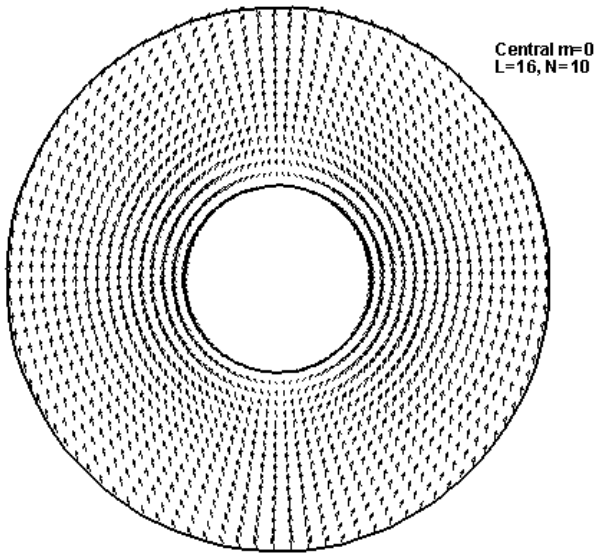

(a)

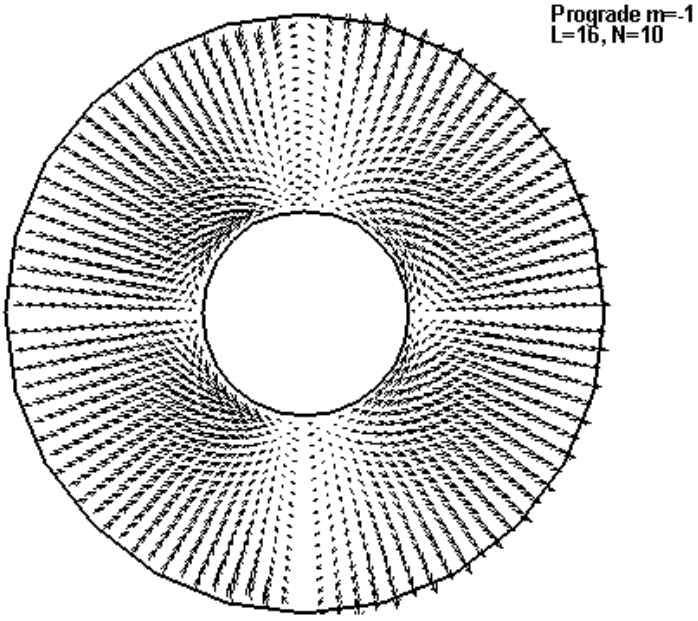

(b)

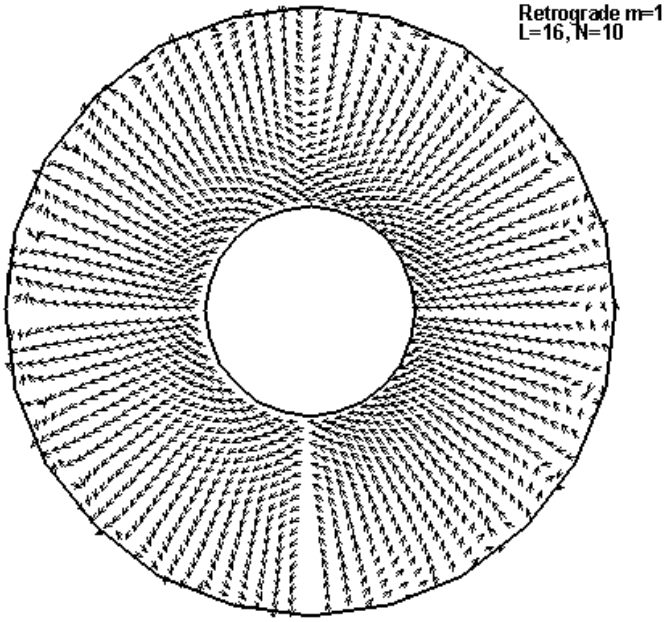

(c)

Figure 4.8 (a-c) shows the displacement patterns for the motion of the fluid in the fluid core during the Slichter oscillations, the so-called Slichter modes. The motion of the inner core for the mode in figure 4.8 (a) is along the z-axis, perpendicular to the figure 4.8 (a), and the fluid motion shows similar patterns. A little disturbance of the boundary conditions near the intersection of the flows, which we believe originates from the effect of a solid body oscillating along z-axis. Therefore, we can report this type of flow to the displacement associated of the inner core moving up and down along the axis of rotation, as it is expected.

Figure 4.8(b) represents the prograde motion of the inner core oscillations associated with the azimuthal number $m = -1$. It shows the fluid flowing through the meridional plane from the left to the right hand side. Figure 4.18(c) shows the flow of the fluid due to the displacement of the inner core for the azimuthal number $m = 1$. As in figure 4.9(b), this flow is directed from the right to the left hand side. For these two modes, the motion of the inner core is horizontal. The displacement vectors in the fluid core clearly follow the motion of the inne core. Moreover, the overall displacement patterns are different in direction and structure, therefore supporting the non-symmetry of these modes.

To compute σ for the Slichter modes, we have used a minimun of $3 \times 10 \times 16 = 480$ terms. The error involved in adding the terms for the complexity of the Legendre polynomial is the main cause of the small discrepancy in the plot of the eigenfunctions. It may appear that near the inner core boundary, the boundary conditions are not satisfied. However, recall that these are the displacement vectors for the translational motion of the inner core. It is expected that the fluid motion is in the direction of the inner core motion.

Chapter 5

CONCLUSIONS

A great effort to detect the Slichter and other core oscillations of the Earth has been made in the past few decades. This is due to the development of a superconducting gravimeter network distributed globally. In this study, the frequencies and displacement eigenfunctions of some of the low order inertial modes and the Slichter modes are computed numerically using a realistic Earth model. A Galerkin method is implemented for the numerical integration of the dynamics of the fluid core, and the inner core equations of motion. The boundary conditions were implemented in a convenient way. The periods of the Slichter triplet were found to be 5.25403, 4.97651 and 5.87529 hours associated to the central ($m = 0$), retrograde ($m = 1$) and prograde ($m = 1$) modes for a realistic spherical Earth model. These results provide a theoretical reference for possible identification and also for future observations.

The results of this work were achieved by following a number of steps which can be summarized as:

-We solve the 3PD for the dynamics of the fluid core.

-We expand the equations using a spherical harmonic representation of the scalar fields V_1 χ, and ζ, and use the orthogonality relation and the linear independence of the functions to remove the θ and ϕ dependence, so that the final coupled equations are functions of the radial components only.

-We use the natural character of the boundary conditions to reduce the second order derivatives to first order ones.

-The results for the inertial modes of a spherical and neutrally stratified PREM are computed and compared to those previously studied by Seyed-Mahmoud et al. [35], as a test of our program.

-The inner core equations of motion were expanded and added to the 3PD for the final form of the system of equations which needed to be solved numerically for the frequencies of the Slichter modes.

-We made sure of the convergence of the results by increasing the number of terms in both θ and r components.

-We also compute the eigenfunctions for their modes and our results are different by as much as 5%, from those given by Peng [25], and Wu and Rochester [67]. We can attribute the difference to the fact that Peng [25] used an elastic Earth model whereas we use a rigid inner core and mantle. Our results are, however, significantly different from those given by Rieutord [57]. He used a viscous and an incompressible Earth model.

One of the advantages of this method is that we were able to plot the inner core oscillation patterns, which show an oscillating solid body moving up and down for the central mode, and right to left or left to right for the associated prograde and retrograde modes respectively. In future work, the ellipticity of the equipotential surfaces and the elasticity of the solid parts of the Earth may be included.

Appendix A

APPENDIX

A.1 Gradient Operations of the Basis Functions and Scalar Fields

In a sperical coordinate system, and ignoring the ϕ dependence $e^{\pm im\phi}$, we write

$$\nabla(f_{l'}Y_q^{m*}) = \frac{df_{l'}(x)}{dx}P_q^m\widehat{\mathbf{r}} + \frac{1}{x}f_{l'}(x)\frac{dP_q^m}{d\theta}\widehat{\theta} - \frac{im}{x\sin\theta}f_{l'}P_q^m\widehat{\phi} \tag{A.1}$$

Following the same scheme of expansion we write

$$\nabla V_1 = \sum_{n=|m|}^{N}\sum_{l=1}^{L}\left[\frac{df_l(x)}{dx}P_n^m\widehat{\mathbf{r}} + \frac{1}{x}f_l(x)\frac{dP_n^m}{d\theta}\widehat{\theta} - \frac{im}{x\sin\theta}f_lP_n^m\widehat{\phi}\right] \tag{A.2}$$

A.2 Gravity

The gravity at CMB is evaluated as

$$g_0 = G\frac{\int_0^r \rho dV}{r^2} \tag{A.3}$$

We therefore rewrite

$$g_0 = G\frac{M_{IC} + M_{FC}}{r^2} \tag{A.4}$$

where G, M_{IC}, and $M_{FC} = \int_{r_{IC}}^{r} \rho_0 dV$ are the gravitational constant given in chapter 3, the mass of the inner core reported in the code as xM_{IC}, and the mass of the fluid core respectively.

A.3 Density Data

As discussed in chapter 3, here we present the density of the fluid core and the inner core from the PREM data

$$\rho_{FC} = 12.5815 - 1.2638x - 3.6426x^2 - 5.5281x^3 \tag{A.5}$$

$$\rho_{IC} = 13.0885 - 8.8381x^2 \tag{A.6}$$

A.4 Codes to Computes the Inertials and Slichter Modes

In this section, we present the codes used to numerically compute the frequencies and amplitude displacement of both the inertials and Slichter modes of the model of the Earth in this work.

A.4.1 Inertial modes for a rotating and neutrally stratified fluid core of the PREM

The FORTRAN code below computes the (2, 1, 1) mode for the truncation level $L = 5$ and $N = 3$. The flag for the choice of either odd or even modes is given by controlling

lf.

```
Program Inertial2 !!!! IC+beta=0
implicit real*8(a-h,o-z)
parameter(lm=5,nm=3)
PARAMETER (lda=3*lm*nm,ldf=lda,N=lda,ntt=1000)
INTEGER IPVT(N), nout
external dlfdrg,dlftrg,umach
dimension Xmat(lda,lda),FACT(ldf,ldf)
call PREM(x,xrho,xdrho,xalpha,xgzero,xbeta,xGrav)
CALL UMACH (2, NOUT)
write(15,*) 'L=5,N=3'
m=1
lf=2
if(m.eq.0) then
xlm=-0.83d0
else
xlm=0.51d0
endif
Lmax=lm
Nmax=nm
h=1.d0/ntt
dett2=1.0d0
sig=0.498d0
dsig=h
tol=1.d-8
!!!!!!!!!!!!!!!!!!!!!!!!!!!!!!!!!!!!!!!!!!!!!!!!!!!!!!!!
do 321 i=1,10000000
sig=sig+dsig
write(*,*) sig
if(sig.gt.xlm) goto 322
call Pmatrix(Lmax,Nmax,lda,lda,sig, Xmat,lf,m)
if(lf.eq.2.and.m.eq.0) Xmat(1,1)=1.d0
CALL dlftrg (lda,Xmat,lda, FACT, ldf,IPVT)
CALL dlfdrg (lda,FACT,ldf, IPVT, DET1, DET2)
det= DET1*10**DET2
dett=det1*dett2
dett2=det1
if (i.eq.1.or.i.eq.iloop) goto 21
if (dett.lt.0.0d0) then
if (dabs(dsig).le.tol) then
write(*,90) det1, sig
dsig=h
sig=sig-h/2
iloop=i+1
```

```
goto 321
endif
dsig=-dsig/10
goto 321
endif
321 continue
322 continue
90  format(2f14.8)
end
Subroutine Pmatrix(Lmax,Nmax,nl1,nl2,ysig,Xmat,lf,im)
implicit real*8(a-h,o-z)
dimension Xmat(nl1,nl2)
parameter(maxsub=500000)
parameter (ri=1221.5d3,rm=3480.d3,rt=6371.d3)
parameter(xa=ri/rt,xb=rm/rt,x0=-1.d0,x1=1.d0)
external Sq,Sqp2,Sqm2,S2Nq,S2Nqp2,S2Nqm2,DQDAG,UMACH,dq2ag
external SPq,SPPq,SPqp2,SPqm2,SP2Nq,SP2Nqp2,SP2Nqm2,SPoq,SPoNq,SPo2Nq
common /xd/l,lp,iq,sig,m
common/xxx/xxa,xxb
call umach (2, NOUT)
!x0 and x1 are integration boundaries
!!! Initialization of the matrix elements!!!!!!!!!!!!!!!!!!!!!
m=im
xxa=xa
xxb=xb
sig=ysig
do i=1,nl1
do j=1,nl2
Xmat(i,j)=0.d0
enddo
enddo
ml=Lmax*Nmax
!!!!!!!!!!!!!!!
errrel=0.d0
errabs=1.d-8
irule=6
! start forming the matrix
do 100 k=1, Nmax
if (lf.eq.2.and.m.eq.0) iq=2*(k-1) !even modes
if (lf.eq.1.and.m.eq.0) iq=2*(k-1)+1 !odd modes
if (lf.eq.2.and.m.eq.1) iq=2*(k) !even modes
if (lf.eq.1.and.m.eq.1) iq=2*(k-1)+1 !odd modes
do 101 lp=1,Lmax
lmp=Lmax*(k-1)+lp !Equation 1 row  Momentum equation
```

```
llmp=Lmax*(Nmax+k-1)+lp !Equation 2 row  Poisson equation
lmmp=Lmax*(2*Nmax+k-1)+lp !Equation 3 row  Entropy equation
do 102 l=1, Lmax
!!!!!!!!!!!!!!!!!!!!Generating the matrix Xmat
!!==========MOMENTUM EQUATION==========!!
!*********************************************************************
!!!Matrix formation of E[L*(q)+l]
lq=Lmax*(k-1)+l
if ( (lq.ge.1.d0) .and. (lq.le.ml)) then
call dq2ag(Sq,x0,x1,errabs,errrel,irule,result1,errest,maxsub,neval,nsubin,alist,blist,
rlist,elist,iord)
Xmat(lmp,lq)=-result1
endif
!!!!!!!!!!!!!!!!!!!!!!!!!!!!!!!!!!!!!!!!!!!!!!!!!!!!!!!!
lqp2=Lmax*(k)+l
if ( (lqp2.ge.1.d0) .and. (lqp2.le.ml)) then
call dq2ag(Sqp2,x0,x1,errabs,errrel,irule,result2,errest,maxsub,neval,nsubin,alist,blist,
rlist,elist,iord)
Xmat(lmp,lqp2)=result2
endif
!!!!!!!!!!!!!!!!!!!!!!!!!!!!!!!!!!!!!!!!!!!!!!!!!!!!!!!!!!!!!!!
lqm2=Lmax*(k-2)+l
if ((lqm2.ge.1.d0) .and. (lqm2.le.ml)) then
call dq2ag(Sqm2,x0,x1,errabs,errrel,irule,result3,errest,maxsub,neval,nsubin,alist,
blist, rlist,elist,iord)
Xmat(lmp,lqm2)=result3
endif
!!!End forming elements E[L*(q)+l]
!*********************************************************************
!!!Matrix formation of E[L*(N+q)+l]
lqq=Lmax*(Nmax+k-1)+l
if ( (lqq.gt.ml) .and. (lqq.le.2*ml)) then
call  dq2ag(Sq,x0,x1,errabs,errrel,irule,result1,errest,maxsub,neval,nsubin,alist,blist,
rlist,elist,iord)
Xmat(lmp,lqq)=result1
endif
!!!!!!!!!!!!!!!!!!!!!!!!!!!!!!!!!!!!!!!!!!!!!!!!!!!!!!!!
lqpp2=Lmax*(Nmax+k)+l
if ( (lqpp2.gt.ml) .and. (lqpp2.le.2*ml)) then
call dq2ag(Sqp2,x0,x1,errabs,errrel,irule,result2,errest,maxsub,neval,nsubin,alist,blist,
rlist,elist,iord)
Xmat(lmp,lqpp2)=-result2
endif
!!!!!!!!!!!!!!!!!!!!!!!!!!!!!!!!!!!!!!!!!!!!!!!!!!!!!!!!!!!!!!!
```

```
lqmm2=Lmax*(Nmax+k-2)+l
if ( (lqmm2.gt.ml) .and. (lqmm2.le.2*ml)) then
call dq2ag(Sqm2,x0,x1,errabs,errrel,irule,result3,errest,maxsub,neval,nsubin,alist,blist,
rlist,elist,iord)
Xmat(lmp,lqmm2)=-result3
endif
!!!End forming elements E[L*(N+q)+l]
!*****************************************************************************
!!!Matrix formation of E[L*(2N+q)+l]
lqqq=Lmax*(2*Nmax+k-1)+l
if ( (lqqq.gt.2*ml) .and. (lqqq.le.3*ml)) then
call dq2ag(S2Nq,x0,x1,errabs,errrel,irule,result11,errest,maxsub,neval,nsubin,alist,
blist,rlist,elist,iord)
Xmat(lmp,lqqq)=result11
endif
write(*,*) result11
!!!End forming elements E[L*(2N+q)+l]
!!=================END of MOMENTUM EQUATION============!!
!*****************************************************************************
!!=================ENTROPY EQUATION=================!!
!*****************************************************************************
!!!Matrix formation of E[L*(q)+l]
lq=Lmax*(k-1)+l
if ( (lq.ge.1.d0) .and. (lq.le.ml)) then
call dq2ag(SPq,x0,x1,errabs,errrel,irule,result111,errest,maxsub,neval,nsubin,alist,
blist,rlist,elist,iord)
Xmat(lmmp,lq)=result111
endif
!!!!!!!!!!!!!!!!!!!!!!!!!!!!!!!!!!!!!!!!!!!!!!
lqp2=Lmax*(k)+l
if ( (lqp2.ge.1.d0) .and. (lqp2.le.ml)) then
call dq2ag(SPqp2,x0,x1,errabs,errrel,irule,result222,errest,maxsub,neval,nsubin,alist,
blist, rlist,elist,iord)
Xmat(lmmp,lqp2)=result222
endif
!!!!!!!!!!!!!!!!!!!!!!!!!!!!!!!!!!!!!!!!!!!!!!!!!!
lqm2=Lmax*(k-2)+l
if ( (lqm2.ge.1.d0) .and. (lqm2.le.ml)) then
call dq2ag(SPqm2,x0,x1,errabs,errrel,irule,result333,errest,maxsub,neval,nsubin,alist,
blist,rlist,elist,iord)
Xmat(lmmp,lqm2)=result333
endif
!!!End forming elements E[L*(q)+l]
!*************************************************************************
```

```
!!!Matrix formation of E[L*(N+q)+l]
lqq=Lmax*(Nmax+k-1)+l
if ( (lqq.gt.ml) .and. (lqq.le.2*ml)) then
call dq2ag(SPPq,x0,x1,errabs,errrel,irule,result101,errest,maxsub,neval,nsubin,alist,
blist,rlist,elist,iord)
Xmat(lmmp,lqq)=result101
endif
!!!!!!!!!!!!!!!!!!!!!!!!!!!!!!!!!!!!!!!!!!!!!!!!!!!!!!!!!!!!!!!!!!!!!
lqpp2=Lmax*(Nmax+k)+l
if ( (lqpp2.gt.ml) .and. (lqpp2.le.2*ml)) then
call dq2ag(SPqp2,x0,x1,errabs,errrel,irule,result222,errest,maxsub,neval,nsubin,alist,
blist,rlist,elist,iord)
Xmat(lmmp,lqpp2)=-result222
endif
!!!!!!!!!!!!!!!!!!!!!!!!!!!!!!!!!!!!!!!!!!!!!!!!!!!!!!!!!!!!!!!!!!!!!!!!!!!!
lqmm2=Lmax*(Nmax+k-2)+l
if ( (lqmm2.gt.ml) .and. (lqmm2.le.2*ml)) then
call dq2ag(SPqm2,x0,x1,errabs,errrel,irule,result333,errest,maxsub,neval,nsubin,alist,
blist,rlist,elist,iord)
Xmat(lmmp,lqmm2)=-result333
endif
!!!End forming elements E[L*(N+q)+l]
!********************************************************************************************
!!!Matrix formation of E[L*(2N+q)+l]
lqqq=Lmax*(2*Nmax+k-1)+l
if ( (lqqq.gt.2*ml) .and. (lqqq.le.3*ml)) then
call dq2ag(SP2Nq,x0,x1,errabs,errrel,irule,result110,errest,maxsub,neval,nsubin,alist,
blist,rlist,elist,iord)
Xmat(lmmp,lqqq)=result110
endif
!!=======================END of ENTROPY EQUATION============!!
!********************************************************************************************
!!=======================POISSON EQUATION======================!!
!********************************************************************************************
!!!Matrix formation of E[L*(q)+l]
lq=Lmax*(k-1)+l
if ( (lq.ge.1.d0) .and. (lq.le.ml)) then
call dq2ag(SPoq,x0,x1,errabs,errrel,irule,result1110,errest,maxsub,neval,nsubin,alist,
blist,rlist,elist,iord)
Xmat(llmp,lq)=result1110
endif
!!!End forming elements E[L*(q)+l]
!**************************************************************************************
!!!Matrix formation of E[L*(N+q)+l]
```

```
lqq=Lmax*(Nmax+k-1)+l
if( (lqq.gt.ml) .and. (lqq.le.2*ml)) then
call dq2ag(SPoNq,x0,x1,errabs,errrel,irule,result1010,errest,maxsub,neval,nsubin,alist,
blist,rlist,elist,iord)
Xmat(llmp,lqq)=result1010
endif
!!!End forming elements E[L*(N+q)+l]
!!==================END of POISSON EQUATION============!!
!*************************************************************************
102 continue
101 continue
100 continue
end
!!!!!!!!!!!!!!!!FUNCTIONS!!!!!!!!!!!!!!!!!!!!!!!!!!!!
function f(l,x)
implicit real*8(a-h,o-z)
external xgender
f=xgender(l,0,x)
return
end
!!!!!!!!!!!!!!!!DERIVATIVES!!!!!!!!!!!!!!!!!!!!!!!!!!!!
function df(l,x)
implicit real*8(a-h,o-z)
common/xxx/xa,xb
external dxgender
df=2.d0/(xb-xa)*dxgender(l,0,x)
return
end
!!!!!!!!!!!!!!!!!!!!!!!!MOMENTUM EQUATIONS FUNCTIONS!!!!!!!!!!!!!!!!!!!!!!!!!!!!
function Sq(xp)
implicit real*8(a-h,o-z)
common /xd/l,lp,iq,sig,m
common/xxx/xa,xb
external f,df
x=(xb-xa)*xp/2 +(xb+xa)/2
bmq= dfloat( (iq*(iq+1)-3*m*m) )/( (2*iq+3)*(2*iq-1) )
fl=f(l-1,xp)
fp=f(lp-1,xp)
dfl=df(l-1,xp)
dfp=df(lp-1,xp)
Sq=(sig**2)*(x*x*dfl*dfp+iq*(iq+1)*fl*fp)+m*sig*(fl*fp+x*fp*dfl+x*fl*dfp)-
(2.d0*iq*(iq+1)/3-m*m)*fp*fl-x*x*dfl*dfp/3-(2.d0*fl*fp-x*fp*dfl+x*fl*dfp)*bmq-

(2.d0*x*x*dfl*dfp/3+2.d0*x*fp*dfl-2.d0*iq*(iq+1)*fl*fp/3)*bmq
```

```
return
end
!!!!!!!!!!!!!!!!!!!!!!!!!!!!!!!!!!!!!!!!!!!!!!!!!!!!!!!!!!!!!!!!!!!!!!!
function Sqp2(xp)
implicit real*8(a-h,o-z)
common /xd/l,lp,iq,sig,m
common/xxx/xa,xb
external f,df
x=(xb-xa)*xp/2 +(xb+xa)/2
amq2=dfloat((3*(iq+m+2)*(iq+m+1)) )/( 2*(2*iq+5)*(2*iq+3) )
fl=f(l-1,xp)
fp=f(lp-1,xp)
dfl=df(l-1,xp)
dfp=df(lp-1,xp)
Sqp2=amq2*(2.d0*x*x*dfl*dfp/3+2.d0*x*fp*dfl-2.d0*(iq+2)*(iq+3)*fl*fp/3+
2.d0*(iq+3)*(2.d0*fl*fp/3-x*fp*dfl/3+x*fl*dfp/3))
return
end
!!!!!!!!!!!!!!!!!!!!!!!!!!!!!!!!!!!!!!!!!!!!!!!!!!!!!!!!!!!!!!!!!!!!!!!
function Sqm2(xp)
implicit real*8(a-h,o-z)
common /xd/l,lp,iq,sig,m
common/xxx/xa,xb
external f,df
x=(xb-xa)*xp/2 +(xb+xa)/2
cmq2=dfloat( (3*(iq-m)*(iq-m-1)) )/( 2*(2*iq-3)*(2*iq-1) )
fl=f(l-1,xp)
fp=f(lp-1,xp)
dfl=df(l-1,xp)
dfp=df(lp-1,xp)
Sqm2=cmq2*(2.d0*x*x*dfl*dfp/3+2.d0*x*fp*dfl-2.d0*(iq-2)*(iq-1)*fl*fp/3-
2.d0*(iq-2)*(2.d0*fl*fp/3-x*fp*dfl/3+x*fl*dfp/3))
return
end
!!!!!!!!!!!!!!!!!!!!End function of E[L(N+q)+l] and E[L(q)+l]
!************************************************************
!!!!!!!!!!!!!!!!!!!!Function of E[L(2N+q)+l]
function S2Nq(xp)
implicit real*8(a-h,o-z)
parameter (rt=6371.d3,Rotrate=7.292115d-5)
common /xd/l,lp,iq,sig,m
common/xxx/xa,xb
external f,df
x=(xb-xa)*xp/2 +(xb+xa)/2
```

```
fl=f(l-1,xp)
fp=f(lp-1,xp)
S2Nq=sig**2*(sig*sig-1.d0)*x*x*fl*fp
return
end
!!!!!!!!!!!!!!!!!!!!!!!!!End function of E[L(2N+q)+l]
!*********************************************************************
!!!!!!!!!!!!!!!!!!!!!End MOMENTUM FUNCTIONS!!!!!!!!!!!!!!!!!!!!!!!!!!!!!
!=============================================
!!!!!!!!!!!!!!!!!!!!! ENTROPY EQUATION FUNCTIONS!!!!!!!!!!!!!!!!!!!!!!!!!
!*********************************************************************
!!!!!!!!!!!!!!!!!!!!!!!Function of E[L(N+q)+l] and E[L(q)+l]
function SPq(xp) !function of E[L(q)+l]
implicit real*8(a-h,o-z)
parameter (rt=6371.d3,Rotrate=7.292115d-5)
common /xd/l,lp,iq,sig,m
common/xxx/xa,xb
external f,df
x=(xb-xa)*xp/2 +(xb+xa)/2
bmq= dfloat( (iq*(iq+1)-3*m*m) )/( (2*iq+3)*(2*iq-1) )
call PREM(x,rho,drho,alpha,gzero,beta,Grav)
fl=f(l-1,xp)
fp=f(lp-1,xp)
dfl=df(l-1,xp)
dfp=df(lp-1,xp)
g0=gzero/(4.d0*rt*Rotrate*Rotrate) !dimensionless gravity
SPq=-g0*( (sig**2-1.d0/3)*x*x*fp*dfl+m*sig*x*fl*fp-
2.d0*x*x*fp*dfl*bmq/3-x*fl*fp*bmq)
return
end
!!!!!!!!!!!!!!!!!!!!!!!!!!!!!!!!!!!!!!!!!!!!!!!!!!!
function SPPq(xp) !function of E[L(N+q)+l]
implicit real*8(a-h,o-z)
parameter (rt=6371.d3,Rotrate=7.292115d-5)
common /xd/l,lp,iq,sig,m
common/xxx/xa,xb
external f,df
x=(xb-xa)*xp/2 +(xb+xa)/2
bmq= dfloat( (iq*(iq+1)-3*m*m) )/( (2*iq+3)*(2*iq-1) )
call PREM(x,rho,drho,alpha,gzero,beta,Grav)
fl=f(l-1,xp)
fp=f(lp-1,xp)
dfl=df(l-1,xp)
dfp=df(lp-1,xp)
```

```
g0=gzero/(4.d0*rt*Rotrate*Rotrate) !dimensionless gravity
SPPq= g0*( (sig**2-1.d0/3)*x*x*fp*dfl+m*sig*x*fl*fp-
2.d0*x*x*fp*dfl*bmq/3-x*fl*fp*bmq)-sig**2*(sig**2-1.d0)*x*x*fp*fl
return
end
!!!!!!!!!!!!!!!!!!!!!!!!!!!!!!!!!!!!!!!!!!!!!!!!
function SPqp2(xp) !function of E[L(N+q+2)+l]
implicit real*8(a-h,o-z)
parameter (rt=6371.d3,Rotrate=7.292115d-5)
common /xd/l,lp,iq,sig,m
common/xxx/xa,xb
external f,df
x=(xb-xa)*xp/2 +(xb+xa)/2
amq2=dfloat((3*(iq+m+2)*(iq+m+1)) )/( 2*(2*iq+5)*(2*iq+3) )
call PREM(x,rho,drho,alpha,gzero,beta,Grav)
fl=f(l-1,xp)
fp=f(lp-1,xp)
dfl=df(l-1,xp)
dfp=df(lp-1,xp)
g0=gzero/(4.d0*rt*Rotrate*Rotrate) !dimensionless gravity
SPqp2=g0*amq2*(2.d0*x*x*fp*dfl/3+2.d0*(iq+3)*x*fl*fp/3)
return
end
!!!!!!!!!!!!!!!!!!!!!!!!!!!!!!!!!!!!!!!!!!!!!!!!
function SPqm2(xp) !function of E[L(N+q-2)+l]
implicit real*8(a-h,o-z)
parameter (rt=6371.d3,Rotrate=7.292115d-5)
common /xd/l,lp,iq,sig,m
common/xxx/xa,xb
external f,df
x=(xb-xa)*xp/2 +(xb+xa)/2
cmq2=dfloat( (3*(iq-m)*(iq-m-1)) )/( 2*(2*iq-3)*(2*iq-1) )
call PREM(x,rho,drho,alpha,gzero,beta,Grav)
fl=f(l-1,xp)
fp=f(lp-1,xp)
dfl=df(l-1,xp)
dfp=df(lp-1,xp)
g0=gzero/(4.d0*rt*Rotrate*Rotrate) !dimensionless gravity
SPqm2=g0*cmq2*(2.d0*x*x*fp*dfl/3-2.d0*(iq-2)*x*fl*fp/3)
return
end
!!!!!!!!!!!!!!!!End function of E[L(N+q)+l] and E[L(q)+l]
!*****************************************************************
!!!!!!!!!!!!!!! function of E[L(2N+q)+l]
```

```
function SP2Nq(xp)
implicit real*8(a-h,o-z)
parameter (rt=6371.d3,Rotrate=7.292115d-5)
common /xd/l,lp,iq,sig,m
common/xxx/xa,xb
external f,df
x=(xb-xa)*xp/2 +(xb+xa)/2
bmq= dfloat( (iq*(iq+1)-3*m*m) )/( (2*iq+3)*(2*iq-1) )
call PREM(x,rho,drho,alpha,gzero,beta,Grav)
fl=f(l-1,xp)
fp=f(lp-1,xp)
alf=alpha/(2.d0*rt*Rotrate) !alf is the dimensionless p-wave
SP2Nq= -(alf**2)*sig*sig*(sig*sig-1.d0)*x*x*fl*fp
return
end
!!!!!!!!!!!!!!!!!!!!!!End ENTROPY EQUATION FUNCTIONS!!!!!!!!!!!!!!!!!!!!!!!!
!=============================================
!!!!!!!!!!!!!!!!!!!!!!POISSON EQUATION FUNCTIONS!!!!!!!!!!!!!!!!!!!!!!!!!!!
!*************************************************************
!!!!!!!!!!!!!!!!!!!!!!function of E[L(q)+l]
function SPoq(xp)
implicit real*8(a-h,o-z)
common /xd/l,lp,iq,sig,m
common/xxx/xa,xb
external f,df
x=(xb-xa)*xp/2 +(xb+xa)/2
bmq= dfloat( (iq*(iq+1)-3*m*m) )/( (2*iq+3)*(2*iq-1) )
fl=f(l-1,xp)
fp=f(lp-1,xp)
dfl=df(l-1,xp)
dfp=df(lp-1,xp)
SPoq=x*x*dfp*dfl+iq*(iq+1)*fl*fp
return
end
!!!!!!!!!!!!!!!!!!!!!!!!End function of E[L(q)+l]
!***********************************************************
!!!!!!!!!!!!!!!!!!!!function of E[L(N+q)+l]
function SPoNq(xp)
implicit real*8(a-h,o-z)
parameter(pi=3.14159265d0)
parameter (rt=6371.d3,Rotrate=7.292115d-5)
common /xd/l,lp,iq,sig,m
common/xxx/xa,xb
external f,df
```

```
x=(xb-xa)*xp/2 +(xb+xa)/2
amq2=dfloat((3*(iq+m+2)*(iq+m+1)) )/( 2*(2*iq+5)*(2*iq+3) )
call PREM(x,rho,drho,alpha,gzero,beta,Grav)
fl=f(l-1,xp)
fp=f(lp-1,xp)
alf=alpha/(2.d0*rt*Rotrate) !alf is the dimensionless p-wave
SPoNq=-4.d0*pi*Grav*x*x*fl*fp/alf**2
return
end
!!!!!!!!!!!!!!!!!!!!!!!!End function of E[L(N+q)+l]
!!!!!!!!!!!!!!!!!!!!End POISSON EQUATION FUNCTIONS!!!!!!!!!!!!!!!!!!!!!!
!==========================================
!!!!!!!!!! Material profiles of PREM
Subroutine PREM(x,xrho,xdrho,xalpha,xgzero,xbeta,xGrav) ! PREM with solid
inner core
implicit real*8(a-h,o-z)
parameter (ri=1221.5d3,rm=3480.d3,rt=6371.d3,xa=ri/rt,xb=rm/rt)
parameter(c1=11.0487d3,c2=-4.0362d3,c3=4.8023d3,c4=-13.5732d3)!PREM con-
stant
parameter(a1=12.5815d3,a2=-1.2638d3,a3=-3.6426d3,a4=-5.5281d3,xMic=2425084894.30688d0)
parameter(pi=3.14159265d0,Rotrate=7.292115d-5,GC=6.6690941d-11)
xalpha=c1+c2*x+c3*x*x+c4*x**3
xrho=a1+a2*x+a3*x*x+a4*x*x*x ! density
xdrho=a2+2*a3*x+3*a4*x**2 ! derivative of density
xgzero= GC*(xMic + 4*pi*rt*( (a1/3.d0)*(x**3- xa**3) + (a2/4.d0)*(x**4-
xa**4) +
(a3/5.d0)*(x**5- xa**5)+ (a4/6.d0)*(x**6- xa**6)) )/(x*x) !gravity
xbeta=0.d0
!xbeta= 1.d0+xalpha*xalpha/xrho/xgzero*xdrho/rt
xGrav=(GC*xrho)/(4*Rotrate**2) ! evaluate the dmensionless G in poisson
equation
end subroutine
!!!!!!!!!!!!!!!!!!!!!!!!!
!!!**********Associated Legendere polynomials**********!!!!!!!!!!!!!!!!!!!!!!!!
function xgender(l,m,x)
implicit real*8(a-h,o-z)
if (m.lt.0.or.m.gt.l.or.dabs(x).gt.1.d0) pause 'bad argument'
pmm=1.d0
if (m.gt.0) then
somx2=dsqrt((1.d0-x)*(1.d0+x))
fact=1.d0
do 11 i=1,m
pmm=-pmm*fact*somx2
fact=fact+2.d0
```

```
11 continue
endif
if (l.eq.m) then
plgndr=pmm
else
pmmp1=x*(2*m+1)*pmm
if(l.eq.m+1) then
plgndr=pmmp1
else
do 12 ll=m+2,l
pll=(x*(2*ll-1)*pmmp1-(ll+m-1)*pmm)/(ll-m)
pmm=pmmp1
pmmp1=pll
12 continue
plgndr=pll
endif
endif
xgender=plgndr
return
end
!!!!**********Derivatives of the associated Legendere polynomials**********!!!!!!!!!!!!!!!!!!!!
function dxgender(l,m,x)
implicit real*8(a-h,o-z)
if (m.lt.0.or.m.gt.l.or.dabs(x).gt.1.) pause 'bad argument'
pmm=1.d0
dpmm=0.d0
if (m.gt.0) then
somx2=dsqrt(1.d0-x*x)
dsomx2=-x/dsqrt(1.-d0x*x)
fact=1.d0
do 11 i=1,m
dpmm=-fact*(dpmm*somx2+pmm*dsomx2)
pmm=-pmm*fact*somx2
fact=fact+2.d0
11 continue
endif
if (l.eq.m) then
pgender=pmm
dxgender=dpmm
else
pmmp1=x*(2*m+1)*pmm
dpmmp1=(2*m+1)*(pmm+x*dpmm)
if (l.eq.m+1) then
pgender=pmmp1
```

```
dxgender=dpmmp1
else
do 12 ll=m+2,l
dpll=((2*ll-1)*(pmmp1+x*dpmmp1)-(ll+m-1)*dpmm)/(ll-m)
pll=(x*(2*ll-1)*pmmp1-(ll+m-1)*pmm)/(ll-m)
pmm=pmmp1
dpmm=dpmmp1
pmmp1=pll
dpmmp1=dpll
12 continue
pgender=pll
dxgender=dpll
endif
endif
return
end
```

A.4.2 Slichter modes for a rotating and neutrally stratified fluid core of the PREM

To compute the Slichter modes, the code above is considered as a subroutine to generate the coefficients of the matrix of size $3 \times N \times L$ by $3 \times N \times L$ discussed in the matrix generation section in chapter 4. However, for the complete set of the matrix of size $3 \times N \times L + 3$ by $3 \times N \times L + 3$, we will add the subroutine involved for the boundary conditions and inner core equation of motion. Note that in case one wants to test this code, they will have to add the subroutine above for the call of Pmatrix.

```
Program Mode_m1  !!!! Slichter mode for m=1
implicit real*8(a-h,o-z)
parameter(lm=20,nm=10) !
PARAMETER ( lda=3*lm*nm+3, ldf=lda,N=lda,ntt=40)
parameter(pi=3.14159265d0,Rotrate=7.292115d-5)
INTEGER IPVT(N), nout
external dlfdrg,dlftrg,umach
```

```
common/xxx/xxa,xxb
dimension Smat(lda,lda),FACT(ldf,ldf),BCmat(lda,lda),sICmat(lda,lda),Xmat(lda,lda)
character*50 fln
CALL
UMACH (2, NOUT)
write(15,*) 'm=1,L=15 and N=10'
m=1
lf=1
sb=6.d0
Lmax=lm
Nmax=nm
h=1.d0/ntt
do ii=1,lda
do ji=1,lda
Smat(ii,ji)=0.d0
enddo
enddo
!!!!!!!!!!!
dett2=1.0d0
sig=1.5d0
dsig=h
tol=1.d-7
!!!!!!!!!!!!!!!!!!!!!!!!!!!!!!!!!!!!!!!!!!!!!!!!!!!!!!!!!!!!!!!!!!!!!!!
do 321 i=1,20000000
sig=sig+dsig
write(*,*) sig
if(sig.ge.sb) goto 322
call Pmatrix(Lmax,Nmax,lda,lda,sig, Xmat,lf,m)
call Bondcond(Lmax,Nmax,lda,sig,BCmat,lf,m)
call xICmatrix(Lmax,Nmax,lda,sig,sICmat,lf,m)
do ip=1,lda
do ir=1,lda
Smat(ip,ir)=Xmat(ip,ir)+BCmat(ip,ir)+sICmat(ip,ir)
enddo
enddo
CALL dlftrg (lda,Smat,lda, FACT, ldf,IPVT)
CALL dlfdrg (lda,FACT,ldf, IPVT, DET1, DET2)
det= DET1*10**DET2
dett=det1*dett2
dett2=det1
if (i.eq.1.or.i.eq.iloop) goto 321
if (dett.lt.0.0d0) then
if (dabs(dsig).le.tol) then
t=pi/(Rotrate*sig)/3600
```

```
write(*,90) sig, t
dsig=h
sig=sig-h/2
iloop=i+1
goto 321
endif
dsig=-dsig/10
goto 321
endif
321 continue
322 continue
90  format(2f14.6)
end
!!!***********************************************!
Subroutine  xICmatrix(Lmax,Nmax,nl,ysig,sICmat,lf,im)
implicit real*8(a-h,o-z)
dimension (nl,nl)
parameter (ri=1221.5d3,rm=3480.d3,rt=6371.d3)
parameter(xa=ri/rt,xb=rm/rt,x0=-1.d0,x1=1.d0)
parameter(pi=3.14159265d0,Rotrate=7.292115d-5,GC=6.6690941d-11)
external  UMACH,f
common /xd/l,lp,iq,sig,m
common/xxx/xxa,xxb
call  umach (2, NOUT)
m=im
xxa=xa
xxb=xb
sig=ysig
do i=1,nl
do j=1,nl
sICmat(i,j)=0.d0
enddo
enddo
call  Evar(ro,roIC,xk,eta,xlbd)
ml=Lmax*Nmax
k=1
do 300 il=1,201
xp=-1.d0+(il-1)*del
x=(xb-xa)*xp/2 +(xb+xa)/2
do 301 l=1, Lmax
!!!!!!!!!!!!!!!!!!!!Generating the matrix Xmat
!!!!!!!!!!!!!!!!INNER CORE EQUATION !!!!!!!!!!!!!!!!!!!!!!!!!!!!!!!!!!!!!!
!!!Matrix formation of E[L*(q)+l]
lq=Lmax*(k-1)+l
```

```
if ( (lq.ge.1.d0) .and. (lq.le.ml)) then
fl=f(l-1,xp)
res1= 4.d0*fl/xa !
sICmat(3*ml+2,lq)=res1
endif
!!!End formation  E[L*(q)+l]
!*****************************************
!!!Matrix formation of E[L*(Nmax+q)+l]
lqq=Lmax*(Nmax+k-1)+l
if ( (lqq.ge.ml) .and. (lqq.le.2*ml)) then
fl=f(l-1,xp)
res2=-4.d0*xk*fl/xa
sICmat(3*ml+2,lqq)=res2
endif
sICmat(3*ml+1,3*ml+1)=xlbd-eta-sig-sig**2
sICmat(3*ml+1,3*ml+2)=xlbd-eta+sig-sig**2
sICmat(3*ml+2,3*ml+1)=sig-xlbd+eta+sig**2
sICmat(3*ml+2,3*ml+2)=sig+xlbd-eta-sig**2
sICmat(3*ml+3,3*ml+3)=xlbd-sig**2
!!!End INNER CORE EQUATION
!*********************************************
301 continue
300  continue
end
!!!!!!!!!!*********************************************
Subroutine Bondcond(Lmax,Nmax,nl,ysig,BCmat,lf,im)
implicit real*8(a-h,o-z)
dimension BCmat(nl,nl)
parameter (ri=1221.5d3,rm=3480.d3,rt=6371.d3)
parameter(xa=ri/rt,xb=rm/rt,x0=-1.d0,x1=1.d0)
parameter(pi=3.14159265d0,Rotrate=7.292115d-5,GC=6.6690941d-11)
external UMACH,f
common /xd/l,lp,iq,sig,m
common/xxx/xxa,xxb
call umach (2, NOUT)
!!! Initialization of the matrix elements!!!!!!!!!!!!!!!!!!!!
m=im
xxa=xa
xxb=xb
sig=ysig
do i=1,nl
do j=1,nl
BCmat(i,j)=0.d0
enddo
```

```
enddo
ml=Lmax*Nmax
!!!!!!!!!!!!!!!!!!!!!!!!!!!!!!!!!!!!!!!!
errrel=0.d0
errabs=1.d-6
irule=6
del=0.01d0
k=1
do 200 il=1,201
xp=-1.d0+(il-1)*del
x=(xb-xa)*xp/2 +(xb+xa)/2
do 201 lp=1,Lmax
lmp=Lmax*(k-1)+lp  !Momentum BC
llmp=Lmax*(Nmax+k-1)+lp  !Poisson BC
do 202 l=1,Lmax
!!====================MOMENTUM EQUATION=============
fp=f(lp-1,xp)
BCmat(lmp,3*ml+1)=-0.5d0*sig*(sig**2-1.d0)*x*x*fp
BCmat(lmp,3*ml+2)=0.5d0*sig*(sig**2-1.d0)*x*x*fp
!!==================END of MOMENTUM EQUATION=========
!!==================POISSON EQUATION================
GCp=GC/(4.d0*Rotrate**2)
fp=f(lp-1,xp)
call  Evar(ro,roIC,xk,eta,xlbd)
BCmat(llmp,3*ml+1)=-2.d0*pi*GCp*(ro-roIC)*x*x*fp
BCmat(llmp,3*ml+2)=2.d0*pi*GCp*(ro-roIC)*x*x*fp
202 continue
201 continue
200 continue
end
!================================================
Subroutine Evar(ro,roIC,yk,eta,xlbd) !
implicit real*8(a-h,o-z)
parameter (ri=1221.5d3,rm=3480.d3,rt=6371.d3,xa=ri/rt,xb=rm/rt)
parameter(a1=12.5815d3,a2=-1.2638d3,a3=-3.6426d3,a4=-5.5281d3)
parameter(h1=13.0885d3,h2=-8.8381d3)
parameter(pi=3.14159265d0,Rotrate=7.292115d-5,GC=6.6690941d-11)
ro=a1+a2*xa+a3*xa**2+a4*xa**3 ! FC density near ICB
roIC= h1+h2*xa**2 ! IC density at ICB
yk=ro/roIC
eta= (1.d0-yk)/4
xlbd =(pi*GC*(1.d0-yk)*ro)/(3.d0*Rotrate**2)
end subroutine
!!!!!!!******* END******!!!!!!!!!!
```

A.5 Recurrence Chain

The recurrence chains given below are useful for the expansion of the 3PD when the effect of the ellipticity is added. Assuming that we have

$$P_2 P_n^m E[L(n)+l] = (A_n^m P_{n-2}^m + B_n^m P_n^m + C_{n+2}^m) E[L(n)+l] \tag{A.7}$$

since the summation is all over n, we can therefore write

$$P_2 P_n^m E[L(n)+l] = (A_{n+2}^m E[L(n+2)+l] + B_n^m E[L(n)+l] + C_{n-2}^m E[L(n-2)+l]) \tag{A.8}$$

in which A_n^m, B_n^m and C_n^m are the parameters defined in chapter 2. Following the same procedure, we can write

$$(P_2)^2 P_n^m = (A_{n+4}^m A_{n+2}^m + A_{n+2}^m (B_{n+2}^m + B_n^m) + [A_n^m C_{n-2}^m + (B_n^m)^2 + A_{n+2}^m C_{n-2}^m] \tag{A.9}$$
$$+ C_{n-2}^m (B_n^m + B_{n-2}^m) + C_{n-4}^m C_n^m) P_n^m$$

$$P_2 P_2^1 \frac{P_n^m}{d\theta} = (2(n+5) A_{n+4}^m A_{n+2}^m + A_{n+2}^m (3B_{n+2}^m + 2(n+3) B_n^m) + [2(n+1) A_n^m C_{n-2}^m \tag{A.10}$$
$$+ 3(B_n^m)^2 - 2n A_{n+2}^m C_{n-2}^m] + C_{n-2}^m (3B_{n-2}^m - 2(n-2) B_n^m) - 2(n-4) C_{n-4}^m C_n^m) P_n^m$$

A.6 Integrations of the Associated Legendre Polynomial

Below are the necessary integrations for the study of the inertial and also the Slichter modes by adding the effect of the ellipticity.

$$\int \sin^2\theta \frac{dP_n^m}{d\theta} \frac{dP_q^m}{d\theta} \sin\theta d\theta = \int [\; < \frac{2}{3} q(q+1)(1-P_2) - m^2 > P_n^m \tag{A.11}$$
$$\frac{2}{3} P_2^1 \frac{dP_n^m}{d\theta}] P_q^m \sin\theta d\theta$$

$$\int \frac{cos\theta}{\sin\theta}[P_q^m \frac{dP_n^m}{d\theta} + P_n^m \frac{dP_q^m}{d\theta}] \sin\theta d\theta = \int P_n^m P_q^m \sin\theta d\theta \tag{A.12}$$

$$\int \sin^2\theta [P_2 \frac{dP_n^m}{d\theta}\frac{dP_q^m}{d\theta}] \sin\theta d\theta = -\int [\frac{2}{3}(1-2P_2)P_2^1 \frac{dP_n^m}{d\theta} \tag{A.13}$$
$$-P_2 < \frac{2}{3}q(q+1)(1-P_2) - m^2 > P_n^m] P_q^m \sin\theta d\theta$$

$$\int P_2 P_2^1 P_n^m \frac{dP_q^m}{d\theta} \sin\theta d\theta = -\int [2P_2 - 10(P_2)^2 + 2P_q^m + P_2 P_2^1 \frac{dP_n^m}{d\theta}] P_q^m \sin\theta d\theta \tag{A.14}$$

$$\int P_2 \frac{\cos\theta}{\sin\theta}[P_n^m \frac{dP_q^m}{d\theta} + P_q^m \frac{dP_n^m}{d\theta}] \sin\theta d\theta = \int (3P_2+1) P_n^m P_q^m \sin\theta d\theta \tag{A.15}$$

$$\int P_2 [\frac{P_n^m}{\theta} \frac{dP_q^m}{d\theta} + \frac{m^2}{\sin^2\theta} P_q^m P_n^m] \sin\theta d\theta = \int [q(q+1 P_2 P_n^m - P_2^1 \frac{dP_n^m}{d\theta}] P_q^m \sin\theta d\theta \tag{A.16}$$

Bibliography

[1] M. Drinkwater, Y. Kerr, J. Font and M. Berger. Exploring the water cycle of the 'Blue Planet': The Soil Moisture and Ocean (SMOS) mission. *ESA Bulletin*, 157:6–15, 2009.

[2] O. Jensen, D. J. Crossley and J. Hinderer. Atmospheric pressure as a natural climate regulator for a terrestrial planet with a biosphere. *Procededings of the National Scademy of Sciences*, 106:9576–9579, 2009.

[3] A. Cazenave. Geoid, Topography and Distribution of Landforms". in Global Earth physics handbook of physical constant by Ahrens, Thomas. *CGU ISBN 0-87590-851-9*, 1995.

[4] D. D. McCarthy and P. Gerard. Rotational and Elliptical Splitting of the Free Oscillation of the Earth. *IERS Technical Note*, 32, 2003.

[5] J. W. Morgan and E. Anders . Chemical composition of Earth, Venus, and Mercury. *Proceedings of the Academy of Sciences*, 77:6973–6977, 1980.

[6] D. G. Milbert and D. A. Smith. Converting GPS Height into NAVD88 Elevation with the GEOID96 Geoid Height Model. *National Geodetic Survey, NOAA*, 2007.

[7] D. T. Sandwell and W.H. F. Smith. Exploring the Ocean Basins with Satellite Altimeter Data. *National Geodetic Survey, NOAA*, 2006.

[8] Don. L. Anderson. The Inner Core of the Earth. In *Proc. Natl. Acad. Sci. USA*, pages 13966–13968, 2002.

[9] B. A. Bolt. *Inside the Earth: Evidence from Earthquakes.* W.H. Freeman and Company, 1982.

[10] R. Deguen. Structure and Dynamics of Earth's Inner Core. *Earth and Planet. Sci. Lett.*, 333-334:211–225, 2012.

[11] Jeroen Tromp, Prague, Czech Republic. `http://news.discovery.com/earth/is-the-earths-core-solid.html`.

[12] M. H. P. Bott . *The Interior of the Earth: its structure, constitution and evolution.* Edward Arnold Limited, 1982.

[13] R. E. Sheriff and L. P. Geldart. *Exploration Seismology 2nd ed.* Cambridge University Press, 1995.

[14] J. Milsom. *Field Geophysics: The geological field guide*, volume 25. John Wiley and Sons, 1995.

[15] Note accessed online www.alabamaquake.com/education.html. Earthquake and Seismic Education. 2012.

[16] A. M. Dziewonsky and Don L. Anderson. Preliminary Earth model. *Phys. of the Earth and Planet. Int.*, 25:297–356, 1981.

[17] M. W. McElhinny and W. E. Senanayake. Paleomagnetic evidence for existence of the geomagnetic field 3.5 Ga ago. *Journal of Geophys. Res.*, 85:3523–3528, 1980.

[18] M. G. Rochester, J. A. Jacobs., D. E. Smylie and K. F. Chong. Can Precession Power Geomagnetic Dynamo. *Geophys. J. R. Astr. Soc.*, 43:661–678, 1975.

[19] D. Gubbins. Energetics of the Earth's core. *Journal of Geophysics*, 43:453–464, 1977.

[20] J. Verhoogen. Heat balance of the Earth's core. *Geophys. J.*, 4:276–281, 1961.

[21] S. I. Braginski. Structure of the Flayer and Reasons for Convection in the Earth's core. *Dokl. Akad. Nauk. SSSR., Engl. Transl.,*, 149:8–10, 1963.

[22] R. Widmer; G. Master and F. Gilbert. The Spherical Earth visited. In *Proceeding of the* 17^{th} *International Conference on Mathematical Geophysics*, 1988.

[23] F. Gilbert and A. M. Dziewonski. An application of normal mode theory to the retrieval of structural parameters and source mechanisms for seismic spectra. *Phil. Trans. Res. Soc. Lond.*, A278:187, 1975.

[24] F. Busse. On the Free Oscillation of the Earth's Inner Core. *J. Geophys. Res.*, 79:753–757, 1974.

[25] Z. Peng. *The Slichter Modes in a Realistic Earth Model.* PhD thesis, Memorial University of Newfoundland, 1995.

[26] G. Pavel and W. Jack. The Effect of Phase Transformations at the Inner Core Boundary on the slichter Modes. *Phys. Earth Planet. Int.*, 5214:1–6, 2009.

[27] S. Rosat and Y. Rogister. Excitation of the Slichter mode by Collision with a Meteoroid or Pressure Variations at the Surface and Core Boundaries. *Phys. Earth. Planet. Int.*, 190:25–33, 2012.

[28] D. P. Spiros and A. E. Mahmoud. Least Squares Self-Coherency Analysis of Superconducting Gravimeter Records in Search of these Slichter Triplet. *Phys. Earth Planet. Int.*, 160:108–123, 2007.

[29] L. B. Slichter. The Fundamental Free Mode of the Earth's Inner Core. In *Proc. Nat. Acad. Sci. USA*, volume 47, pages 186–190, 1961.

[30] B. V. Jackson and L. B. Slichter . The Residual daily Earth tides at the South Pole. *Journal of Geophysical Research*, 79:1711–1715, 1974.

[31] P. A. Rydelek and L. Knopoff. Spectral Analysis of Gapped: Search for Mode 1S1 at the South Pole. *Journal of Geophys. Res.*, 89:1899–1902, 1984.

[32] D. J. Crossley. The Excitation of Core Modes by Earthquakes. In *Structure and Dynamics of Earth's Deep Interior eds D.E. Smilye and R. Hide, A.G.U.*, pages 41–50, 1988.

[33] D. J. Crossley, J. Hinderer and H. Legros. On the Excitation, Detection and Damping of Core Modes. *Phys. Earth Planet. Int.*, 69:97–116, 1991.

[34] D. J. Crossley. Eigensolutions and Seismic Excitation of the Slichter Modes Triplet for a Fully Rotating Earth Model . *Eos, Trans. Am. Geophys. Un.*, 73.60, 1992.

[35] B. Seyed-Mahmoud, H. John and S. M. Refah. Inertial Modes of a Compressible Fluid Core Model. *Geophys. Astrophys. Fluid Dyn.*, 101:489–505, 2007.

[36] M. G. Rochester. Normal Modes of a Rotating Self-Gravitating Compressible Stratified Fluid Bodies: The Subseismic Wave Equation. In *Continuum Mechanics and its Applications eds GAC*, pages 797–823, 1989.

[37] B. Seyed-Mahmoud. WOBBLE/NUTATION OF A ROTATING ELLIPSOIDAL EARTH WITH LIQUID OUTER CORE: Implementation of a New Set of Equations Describing Dyanmics of Rotating Fluids. Master's thesis, Memorial University of Newfoundland, 1994.

[38] Z. J. Alterman and C. L. Pekeris. Oscillations of the Earth. In *Proc. Soc. London, A, 252*, pages 80–95, 1959.

[39] M. L. Smith. Wobble and Nutation of the Earth. *Geophys. J. R. Astr. Soc.*, 50:103–140, 1977.

[40] D. E. Smylie and M.G. Rochester. Compressibility, Core Dynamics and the Subseismic Wave Equation. *Phys. of the Earth and Planet. Int.*, 24:308–319, 1981.

[41] S. Friedlander. Stability and Waves in the Earth's Fluid Core. *in Proc. U.S. -Italy Conference on Energy Stability and Convectio, Capri, May 1986, Longman Scientific Press Research Notes in Mathematics, ed. Straughan, B., Longman*, 168:325–345, 1988.

[42] M. G. Rochester and Z. R. Peng. The Slichter Modes of a Rotating Earth: A Test of the Subseimic Approximation. *Geophys. J. Int.*, 113:575–585, 1993.

[43] W. J. Wu and M. G. Rochester. Core Dynamics: The Two Potential Description and a New Variational Principle. *Geophys. J. Int.*, 103:697–706, 1990.

[44] D. J. Crossley and M. G. Rochester. The Subseismic Approximation in Core Dynamics. *Geophys. J. Int.*, 108:502–506, 1992.

[45] B. Seyed-Mahmoud and M. Rochester . Dynamics of Rotating Fluids Described by Scalar Potentials. *Phys. Earth. Planet. Int.*, 156:143–151, 2006.

[46] B. Seyed-Mahmoud and M. Tipper . Gravity and Inertial Modes of Rotating Stars. *Astrophys. Geophys. Fluid Dyn.*, 102:383–395, 2008.

[47] Hough, S. S. The Oscillations of a Rotating Ellipsoidal Shell Containing Fluid. *Phil. Trans. R. Soc. London, A*, 186:469–506, 1895.

[48] Poincare, H. Sur la precession des corps deformable. *Bull. Astronomique*, 27:321–356, 1910.

[49] D. J. Crossley. The Free Oscillation Equations at the Centre of the Earth. *Geophys. J. Res. Astr. Soc.*, 41:153–163, 1975.

[50] M. L. Smith. Translational Inner Core Oscillation of a Rotating Slightly Elliptical Earth. *J. Geophys. Res*, 81:3055–3065, 1976.

[51] F. A. Dahlen and R. V. Sailor. Rotational and Elliptical Splitting of the Free Oscillation of the Earth. *Geophys. J. R. Astr. Soc.*, 58:609–623, 1979.

[52] D. E. Smylie. The Inner Core Translational Triplet and the Density Near Earth's Center. *Science*, 255:1678–1682, 1992.

[53] D. J. Crossley, M. G. Rochester and Z. R. Peng. Slichter Modes and the Love Numbers. *Geophys. Res. Let.*, 41:1679–1682, 1992.

[54] K. F. Li, K. Pahlevan, L. Joseph and Y. L. Yung. Simple Data Decomposition Reveals a Surprinsingly Rich Harmonic Spectrum in Superconducting Gravimeter Data. *Eos, Trans. Am. Geophys. Un*, 73:60, 1992.

[55] J. Hinderer, D. J. Crossley, O. G. Jensen and H. Xu. Gravity Noise Levels and Periodic Signal Observed from a Common 2 Year Analysis of the French and Canadian Superconducting Gravimeters. *Eos, Trans. Am. Geophys. Un*, 73:60, 1992.

[56] N. Courtier, B. Ducarne, J. Goodkind, J. Hinderer, Y. Imanishi, N. Seama, H. Sun, J. Bengert, and D. E. Smylie. Global Superconducting Gravimeter Observations and the Search for the Translational Modes of the Inner Core. *Phys. Earth Planet. Int.*, 117:3–20, 2000.

[57] M. Rieutord. Slichter Modes of the Earth Revisited. *Phys. Earth Planet Int.*, 131:269–278, 2002.

[58] Y. Rogister. Splitting of Seismic-Free Oscillations and of the Slichter Triplet Using the Normal Mode theory of a Rotating Ellipsoidal Earth. *Phys. Earth Planet. Int.*, 140:169–182, 2003.

[59] G. L. Marianne and H. Legros. Fluid Core Dynamics and Degree-one Deformations: Slichter Mode and Geocenter Motions. *Phys. Earth Planet Int.*, 161:150–160, 2007.

[60] A. Ern, and J. L. Guermond. *Theory and Practice of Finite Element.* Springer, 2004.

[61] L. Evans. *Partial Differential Equations.* American Math. Soc., 1998.

[62] K. Atkinson and W. Han. *Theoretical Numerical Analysis: A Functional Analysis Framework.* Springer, 2005.

[63] O. C. Ziekiewicz and K. Morgan. *Finite Elements and Approximation.* John Wiley and Sons, 1982.

[64] Z. Peng. Subseismic Description of the Slichter Modes in a Rotating Earth. Master's thesis, Memorial University of Newfoundland, 1990.

[65] H. P. Greenspan. The Theory of Rotating Fluids. *Cambridge University Press*, 1968.

[66] Rogue Wave Software. *IMSL FORTRAN Numerical Library: Mathematical Functions in Fortran.* www.absoft.com/Support/Documentation/MathV1.pdf.

[67] W. J. Wu and M. G. Rochester. Gravity and Slichter modes of the rotating Earth. *Phys. Earth Planet. Int.*, 87:137–154, 1994.

[68] K. E. Bullen and R. A. W., Haddon. The Ellipticity of Surfaces of Equal Density Inside the Earth. *Phys. Earth Planet. Int.*, 7:199–202, 1973.

[69] F. A. Dahlen and R. V. Sailor. Rotational and Elliptical Splitting of the Free Oscillation of the Earth. *Geophys. J. R. Astr. Soc.*, 58:609–623, 1979.

[70] Z. Kopal. Clairaut Coordinates and Vibrational Stability of Distorded Stars. *Astrophys. Space Sci.*, 70:407–424, 1980.

[71] A. H. Miller. The Figure of the Earth. *J. Roy. Astron. Soc. Canada*, XL:133–138, 1946.

[72] M. L. Smith. The Scalar Equations of Infinitesimal Elastic-Gravitational Motion for a Rotating, Slightly Elliptical Earth. *Geophys. J. R. Astr. Soc.*, 37:491–526, 1974.

[73] D. E. Smylie and L. Mansinha. The Elasticity Theory of Dislocation in Real Earth Model and Charges in the Rotation of the Earth. *Geophys. J. R. Astr. Soc.*, 23:329–354, 1971.

[74] F. D. Stacey. Physics of the Earth. 1969.

[75] D. L. Walter. The Figure of the Earth and the New International Ellipsoid of References. *Science*, 63:242–248, 1926.

[76] Y. Zhang. Free Wobble/Nutation of the Earth: A new Approach for Hydrostatic Earth Models. Master's thesis, Memorial University of Newfoundland, 1998.